PERFORMANCE EVALUATION OF HOMING GUIDANCE LAWS FOR TACTICAL MISSILES

Charles F. Price, et al

Analytic Sciences Corporation

Prepared for:

Office of Naval Research

1 January 1973

TR-170-4

PERFORMANCE EVALUATION OF HOMING GUIDANCE LAWS FOR TACTICAL MISSILES

1 January 1973

TASC

6 JACOB WAY/READING, MASSACHUSETTS 01867 (617) 944-6850

TR-170-4

PERFORMANCE EVALUATION OF HOMING GUIDANCE LAWS FOR TACTICAL MISSILES

1 January 1973

Prepared for the

OFFICE OF NAVAL RESEARCH
AERONAUTICS PROGRAMS, CODE 461
DEPARTMENT OF THE NAVY
ARLINGTON, VIRGINIA 22217

Under

Contract Number N00014-69-C-0391

Prepared by:

Charles F. Price
Ronald S. Warren

Approved by:

Arthur A. Sutherland, Jr.
Arthur Gelb

THE ANALYTIC SCIENCES CORPORATION
6 Jacob Way
Reading, Massachusetts 01867

UNCLASSIFIED

Security Classification

DOCUMENT CONTROL DATA - R & D

(Security classification of title, body of abstract and indexing annotation must be entered when the overall report is classified)

1. ORIGINATING ACTIVITY (Corporate author) The Analytic Sciences Corporation 6 Jacob Way Reading, Massachusetts 01867	2a. REPORT SECURITY CLASSIFICATION Unclassified 2b. GROUP

3. REPORT TITLE

PERFORMANCE EVALUATION OF HOMING GUIDANCE LAWS FOR TACTICAL MISSILES

4. DESCRIPTIVE NOTES (Type of report and inclusive dates)

Technical Report

5. AUTHOR(S) (First name, middle initial, last name)

Charles F. Price
Ronald S. Warren

6. REPORT DATE 1 January 1973	7a. TOTAL NO. OF PAGES 100	7b. NO. OF REFS 15
8a. CONTRACT OR GRANT NO. N00014-69-C-0391 b. PROJECT NO. c. d.	9a. ORIGINATOR'S REPORT NUMBER(S) TR-170-4 9b. OTHER REPORT NO(S) (Any other numbers that may be assigned this report)	

10. DISTRIBUTION STATEMENT

Qualified requestors may obtain copies of this report from DDC.

11. SUPPLEMENTARY NOTES	12. SPONSORING MILITARY ACTIVITY Office of Naval Research Department of the Navy Arlington, Virginia 22217

13. ABSTRACT

A number of homing guidance laws, designed using principles of modern stochastic control theory, are compared using a recently developed analytical technique (CADET) for propagating the statistics of nonlinear, randomly excited systems. The guidance laws include proportional guidance, optimal linear guidance, and optimal nonlinear guidance. Each law is evaluated in a realistic nonlinear model of the missile guidance system and the homing geometry. This work provides a direct comparative evaluation of several important guidance techniques, and extends the usefulness of CADET for analyzing nonlinear guidance systems.

DD FORM 1 NOV 68 1473 REPLACES DD FORM 1473, 1 JAN 64, WHICH IS OBSOLETE FOR ARMY USE.

UNCLASSIFIED

Security Classification

14. KEY WORDS	LINK A		LINK B		LINK C	
	ROLE	WT	ROLE	WT	ROLE	WT
Missile Guidance Optimal Guidance Homing Guidance Terminal Control Nonlinear Stochastic Systems Analysis						

FOREWORD

This report completes a broad research program in new concepts for guidance and control of tactical missiles. Other work performed under this contract is described in: TR-170-1, "Adaptive Control and Guidance for Tactical Missiles"; TR-170-2, "Optimal Stochastic Guidance Laws for Tactical Missiles"; TR-170-3, "Adaptive Control with Explicit Parameter Identification for Tactical Missiles". The authors wish to express appreciation to Mr. David Siegel of the Office of Naval Research for his encouragement and support throughout this investigation.

TABLE OF CONTENTS

		Page No.
FOREWORD		ii
ABSTRACT		iii
List of Figures		vi
List of Tables		ix
1.	INTRODUCTION	1-1
	1.1 Background	1-1
	1.2 Methodology	1-2
	1.3 Organization	1-3
2.	GUIDANCE SYSTEM MODEL	2-1
	2.1 System Dynamics	2-1
	2.2 Missile Guidance Laws	2-6
3.	GUIDANCE SYSTEM EVALUATION	3-1
	3.1 Evaluation Procedure	3-1
	3.2 Simulation Results	3-3
4.	SUMMARY AND CONCLUSIONS	4-1
	4.1 Summary	4-1
	4.2 Conclusions	4-2
APPENDIX A – TRUTH MODEL DEVELOPMENT		A-1
	A.1 Seeker Module	A-1
	A.2 Noise Module	A-10
	A.3 Autopilot Module	A-15
	A.4 Geometry Module	A-21
	A.5 Target Module	A-29
	A.6 Guidance Module	A-32
	A.7 Computational Requirements	A-46

TABLE OF CONTENTS (Continued)

		Page No.
APPENDIX B –	THE COVARIANCE ANALYSIS DESCRIBING FUNCTION TECHNIQUE (CADET)	B-1
B.1	Covariance Analysis for Linear Systems	B-1
B.2	Covariance Analysis for Nonlinear Systems	B-4
B.3	Computation of Describing Functions	B-12
B.4	Mixed Continuous-Discrete Systems	B-15
B.5	Describing Functions for Saturation and Sinusoidal Nonlinearities	B-19
REFERENCES		R-1

LIST OF FIGURES

Figure No.		Page No.
2.1-1	Guidance System Truth Model with Major Subsystems	2-1
2.1-2	Guidance System Mathematical Model	2-5
2.1-3	Intercept Geometry	2-5
2.2-1	Guidance Law A	2-9
2.2-2	Guidance Law B	2-9
2.2-3	Guidance Laws C, D, and E	2-9
3.2-1	Cadet-Monte Carlo Comparison versus Missile Acceleration Capability	3-5
3.2-2	Guidance Law Performance versus Target Maneuver Bandwidth	3-7
3.2-3	Performance of Proportional Guidance Using a Kalman Filter versus a First-Order Filter	3-7
3.2-4	Performance of Proportional Guidance as a Function of the Navigation Ratio	3-9
3.2-5	Guidance Law Performance versus Missile Maneuver Capability	3-9
3.2-6	Guidance Law Performance versus Missile Autopilot Time Constant	3-10
3.2-7	Guidance Law Performance versus Target Maneuver Level	3-11
3.2-8	Guidance Law Sensitivity to Aberration Error; Dominant Autopilot Pole = $-1.0\ \text{sec}^{-1}$	3-12

LIST OF FIGURES (Continued)

Figure No.		Page No.
3.2-9	Guidance Law Sensitivity to Aberration Error; Dominant Autopilot Pole = -3.3 rad/sec	3-13
3.2-10	Guidance Law Sensitivity to Design Value of the Autopilot Time constant	3-14
A.1-1	Seeker-Radome Geometry	A-3
A.1-2	Signal Processing Nonlinearities	A-4
A.1-3	Effect of Aberration Error	A-5
A.1-4	Typical Aberration Angle Error as a Function of Look Angle	A-6
A.1-5	Seeker Subsystem Block Diagram	A-7
A.1-6	Seeker Model with Track Loop	A-9
A.3-1	General Missile Autopilot Configuration	A-16
A.3-2	Linear Autopilot Block Diagram	A-18
A.3-3	Simulation Autopilot Model	A-22
A.4-1	Intercept Geometry	A-22
A.4-2	Relative Missile-Target Geometry Near Intercept	A-27
A.5-1	Poisson Square Wave for Target Acceleration	A-30
A.6-1	Guidance Law A	A-34
A.6-2	Kalman Filter Plant Model	A-34
A.6-3	Kalman Filter Mechanization Diagram	A-38
A.6-4	Comparison of Navigation Ratios for Optimal Linear and Nonlinear Laws	A-45

LIST OF FIGURES (Continued)

Figure No.		Page No.
B.1-1	Illustration of Continuous Representation of Linear Dynamic System Equations	B-2
B.2-1	Block Diagram Interpretation of the Linearizing Approximation	B-5
B.2-2	The Describing Function for a Saturation Nonlinearity (Ref. 12) (a) Saturating Nonlinearity (b) Describing Function	B-9
B.3-1	Example of a Single-State-Input Single-Output Nonlinearity	B-14
B.4-1	An Example of a Mixed Continuous Discrete System	B-16
B.5-1	Describing Function for Saturation with a Gaussian Input	B-20
B.5-2	Describing Function for a Sinusoid with a Gaussion Input	B-21

LIST OF TABLES

Table No.		Page No.
2.2-1	Missile Guidance Laws	2-7
3.2-1	Nominal Conditions	3-4
4.1-1	Missile Guidance Laws	4-1
A.7-1	Approximate Kalman Filter Computer Requirements: Two Three-State Filters	A-48

1. INTRODUCTION

1.1 BACKGROUND

Previous investigations of homing guidance laws for tactical missiles have discussed a number of guidance techniques derived using principles of optimal stochastic control theory (Refs. 1-5), which offer potential improvement over conventional proportional guidance. In the past, comparative evaluations of these guidance laws obtained from computer simulations have generally been based upon simplified linear models of guidance system dynamics. It is found that certain frequently neglected effects, such as limited missile maneuvering capability and dynamic coupling between the missile airframe and its homing seeker, significantly influence missile performance. Although the simplified models are adequate for obtaining qualitative comparisons of performance for different guidance laws, definitive quantitative evaluations require more accurate mathematical representations of the missile-target engagement situation.

The purpose of this study is to provide comparative performance evaluations of several modern guidance laws using a computer simulation based upon a mathematical "truth" model of the guidance system. The model includes descriptions of the following critical and often neglected missile characteristics: autopilot dynamics, acceleration limit, homing seeker dynamics, range dependent seeker noise, geometric nonlinearities, and random target motion. The guidance laws to be

compared include proportional guidance, optimal linear guidance and optimal nonlinear guidance. These laws are derived based upon a simplified "design" model that neglects many of the above effects; then their performance is tested in a simulation of the truth model. This determines the sensitivity of the guidance system to errors in the design assumptions.

1.2 METHODOLOGY

Traditionally the analysis of random effects in a nonlinear system is accomplished using the monte carlo simulation technique. That is, a large number of sample solutions to the randomly excited differential equations of motion are generated by computer, and ensemble averages of the variables of interest are computed. Frequently a large number of trials (e.g., several hundred) are required to obtain a sufficiently accurate estimate of average performance. This procedure is quite expensive in terms of computer running time and, for a complex system, only a few different system configurations can be evaluated within a limited computational budget.

Recently a new approximate analytical technique has been developed for calculating the statistics of nonlinear stochastic systems (Ref. 6). This method, called the Covariance Analysis Describing Function Technique (CADET), yields good agreement with monte carlo results and requires significantly less computer running time. The basic principal of CADET is that the system nonlinearities are linearized using describing function theory; then the statistics of the resulting linearized system model are analyzed using covariance analysis techniques. The saving in computer time arises because only one solution to a matrix

differential (or difference) equation is required to determine the statistics of a given system configuration, as compared with several hundred solutions of the system differential (or difference) equations with the monte carlo method. The CADET technique is attractive for analyzing guidance systems because it permits the investigation of several different guidance laws over a wide range of values of the system parameters. Consequently, the approach taken in this study is to perform most of the guidance system performance evaluations with a CADET computer simulation, validating the latter with a monte carlo simulation in a selected number of cases.

1.3 ORGANIZATION

Chapter 2 of the report outlines the principal features of the simulation truth model and the guidance laws under comparison. Chapter 3 presents simulation results; a summary and list of the major conclusions are given in Chapter 4. Appendix A provides a detailed discussion of the system truth model; the theoretical background for CADET is presented in Appendix B.

2. GUIDANCE SYSTEM MODEL

2.1 System Dynamics

The principal elements of a missile guidance system are indicated in the block diagram of Fig. 2.1-1. This section briefly describes the function of each subsystem, exclusive of the guidance law, and the features included in the simulation model. The missile guidance law is treated in Section 2.2. The reader is referred to Appendix A for more complete details.

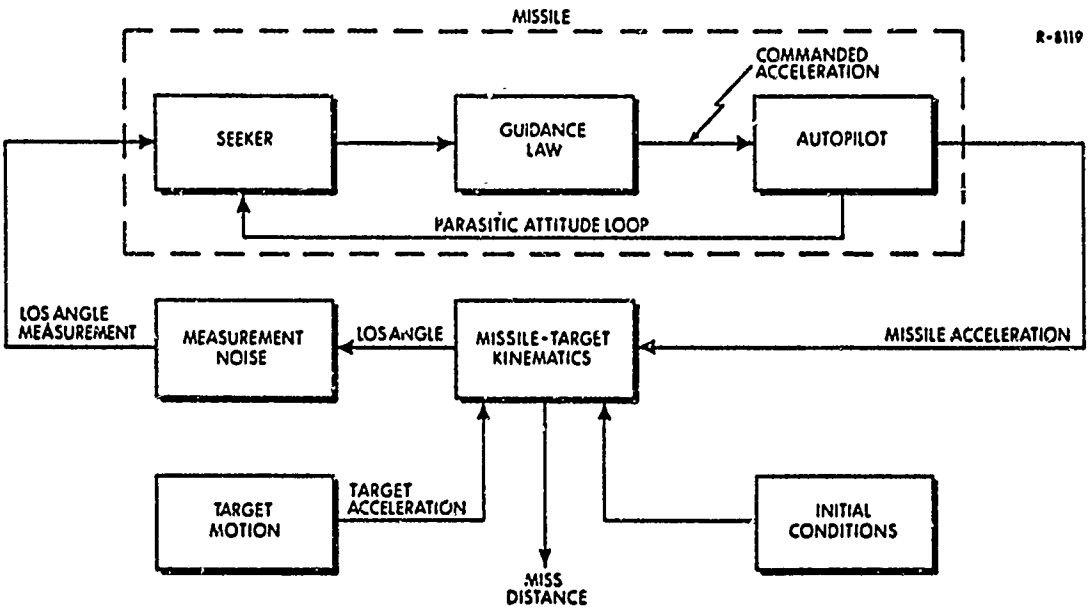

Figure 2.1-1 Guidance System Truth Model with Major Subsystems

Seeker– The homing seeker has the function of tracking the target. Fundamentally it measures the angular position of the line-of-sight (LOS) to the target relative to the sensor centerline by observing the direction of electromagnetic energy reflected from the target (as in a radar seeker) or transmitted by the target (in the case of an infrared or electrooptical seeker). This measured error signal generally serves two functions: first, in the case of a gimballed seeker, the error is used to drive the seeker antenna so as to maintain a small tracking error; this is necessary to prevent losing track of the target. Secondly, the response of the seeker--e.g., its gimbal angle rate, the magnitude of the tracking error, etc.--is used to infer the LOS angular rate, or the LOS angle measured with respect to some reference orientation. Either of these quantities may be used in the guidance law for generating missile acceleration commands which direct the missile toward intercept.

The model of the seeker includes the antenna pointing dynamics, as well as parasitic coupling with the missile airframe. The latter can arise from an error in the direction of the LOS, as perceived by the seeker, caused by aberration of the electromagnetic energy as it passes through the protective covering (radome in the case of a radar) of the missile. This error typically depends upon the missile attitude; therefore the airframe dynamics are coupled to the seeker measurement.

Autopilot – The autopilot refers to the missile airframe dynamics, together with its stability augmentation system. It can be viewed as a servomechanism designed so that its output acceleration follows the input acceleration commands as closely as possible. This study uses two selectable models for the autopilot--one is a first-order lag which provides a first approximation to actual airframe response; the other is a third-order transfer function which more closely represents the dynamics of an actual airframe. In addition, the autopilot model

includes one of the most significant guidance system nonlinearities--an input command limiter which represents the limited maneuvering capability of the airframe.

Missile-Target Kinematics – The model of the missile-target kinematics assumes that the relative closing velocity (range-rate) is constant and that the missile and target accelerations are normal to their respective velocity vectors. This implies that both velocities have constant magnitude but variable direction. The components of missile and target acceleration which are normal to the line-of-sight, and which control the terminal miss distance, are represented as trigonometric functions of the appropriate orientation angles. This constitutes another important nonlinearity included in the model.

Measurement Noise – The noise in the measurement of line-of-sight angle is caused by a number of different error sources, some of which are range dependent. Three types of noise are included in the model: effective receiver noise (decreases with decreasing range), target angular scintillation noise (increases with decreasing range), and range independent noise caused by the seeker servo system and possibly by amplitude fluctuations in the received signal.

Target Motion – The guidance system model includes a provision for a randomly accelerating target. The latter is representative of maneuvers that are constant in magnitude, but switch sign at random times--sometimes referred to as "jinking". The random motion is modeled as the output of a low pass filter driven by white noise; the latter has the same autocorrelation function as the jinking maneuver.

Initial Conditions – A number of initial conditions are specified in the system model which determine the missile trajectory and influence

terminal accuracy. These include:

- Launch Range
- Missile Velocity
- Target Velocity
- Missile Heading Error
- Closing Velocity

For this investigation, most of the above quantities were assigned nominal values that were held fixed throughout the study.

Mathematical models are developed in Appendix A for each of the subsystems indicated in Fig. 2.1-1. Figure 2.1-2 provides a detailed block diagram of the complete guidance system. The missile-target motion is assumed to be restricted to a single plane and the effects of gravity and aerodynamic drag are neglected. The kinematic variables--r_{tm}, v_m, v_t, θ_ℓ, θ_a, θ, a_ℓ, and a_t are defined in Fig. 2.1-3. The quantity k_r is a gain representing the aberration error which dynamically couples the missile airframe motion to the homing seeker. The transfer function coefficients τ_1, λ_t, a_1, a_2, a_3, b_1, b_2, and b_3 are assigned values to yield realistic dynamic characteristics. The switches S_1 and S_2 are positioned according to the type of guidance law being evaluated; their settings are explained in Section 2.2.

One of the more important autopilot parameters is a_3, which combines with k_r in determining the high frequency open loop gain of the parasitic attitude loop; if the latter is excessively large, system instability can result. The value of a_3 tends to increase with missile altitude because a larger missile angle of attack, and hence a higher transient pitch rate, is needed to generate a given acceleration as the air density decreases.

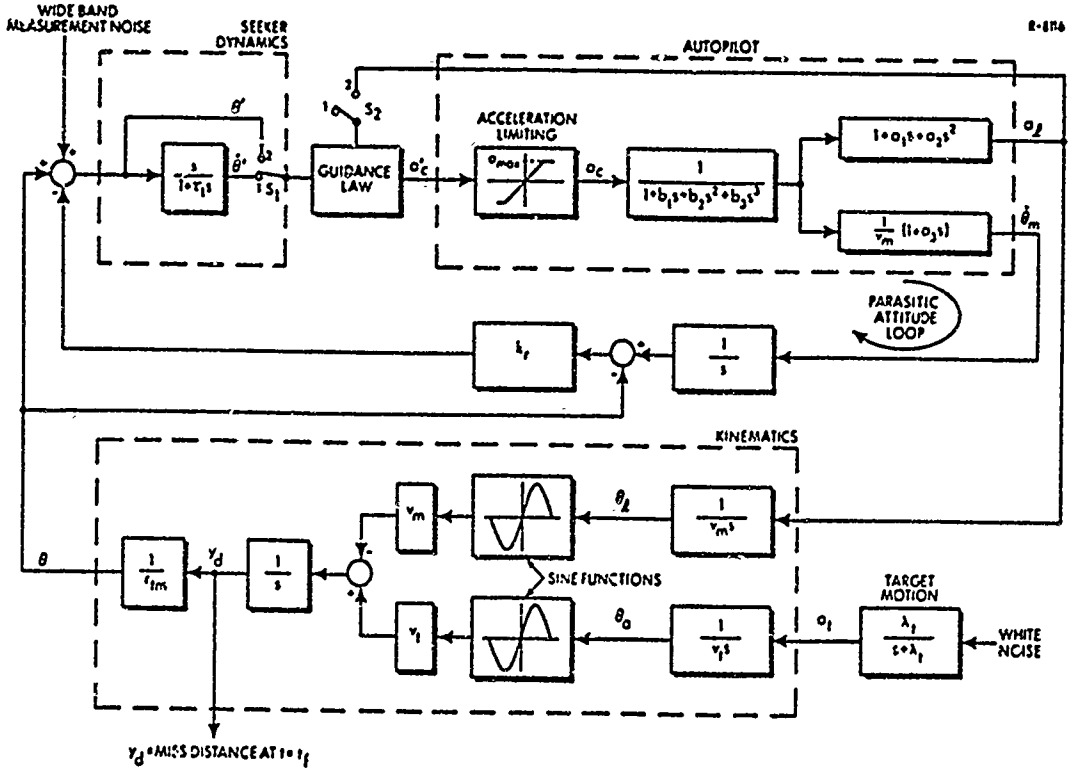

Figure 2.1-2 Guidance System Mathematical Model

R-5083-c

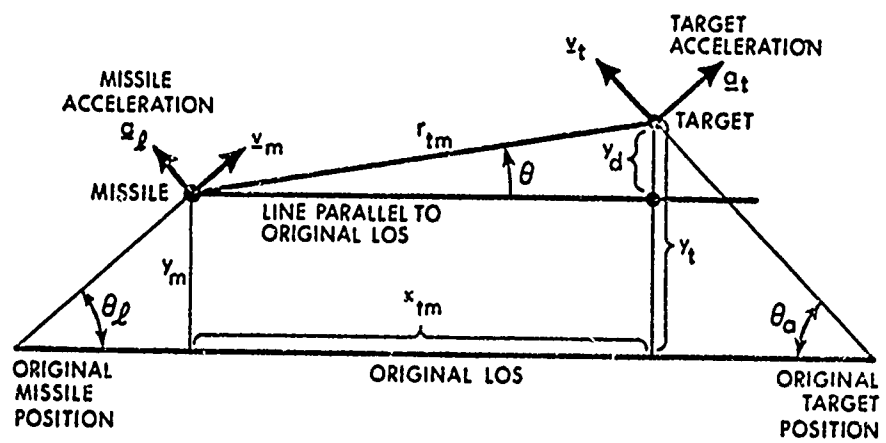

Figure 2.1-3 Intercept Geometry

8

Figure 2.1-2 uses Laplace transform notation to indicate input-output relations associated with linear subsystems. However, the system performance cannot be analyzed in terms of this notation because of the nonlinearities, a time-varying gain ($1/r_{tm}$) and time-varying rms seeker measurement noise. Chapter 3 discusses the methodology used to determine the rms terminal miss distance.

2.2 MISSILE GUIDANCE LAWS

The motivation for this study is partially provided by previous work, described in Ref. 7, which investigated optimal stochastic guidance laws in the presence of missile acceleration limiting, using a limited number of monte carlo simulations and a simplified system model. It was determined that under some circumstances an optimal nonlinear law achieves as much as fifty percent reduction in the miss distance achieved with the linear law. The optimal guidance laws, together with classical guidance methods, provide a hierarchy of techniques that are potentially applicable for tactical missiles, and which need evaluation using a more realistic system model.

Generally speaking, the guidance law is thought of as two cascaded functions -- filtering, or state estimation, and control. The function of the filtering operation is to obtain estimates of those variables needed to mechanize the control law. The latter prescribes the acceleration command according to a policy which will direct the missile trajectory to intercept the target. The methodology used for designing the various laws is discussed in Section A.6. Five different laws are considered; their distinguishing characteristics are summarized in Table 2.2-1.

TABLE 2.2-1

MISSILE GUIDANCE LAWS

Identifying Symbol	Distinguishing Characteristics	Type of Filter
A	Proportional Guidance	First-Order, Low-Pass
B	Proportional Guidance	Kalman
C	Optimal Linear Guidance; Accounts for Target Maneuvers	Kalman
D	Optimal Linear Guidance; Accounts for Target Maneuvers and Missile Autopilot Dynamics	Kalman
E	Optimal Nonlinear Guidance Accounts for Target Maneuvers Missile Autopilot Dynamics, and Missile Airframe Saturation	Kalman

Law A is simply conventional proportional guidance, preceded by a low-pass filter to suppress measurement noise in the sensor output, $\dot{\theta}'$. For this case switches S_1 and S_2 in Fig. 2.1-2 are both in position 1, and the guidance law is mechanized as shown in Fig. 2.2-1, where n' is a specified constant navigation ratio and v_c is the missile-target closing velocity* (range-rate).

Guidance law B uses a Kalman filter to provide an optimal estimate of LOS angular rate, together with the same proportional

*It is assumed that the errors in measuring v_c, r_{tm}, and a_ℓ are negligible. This is a reasonable assumption in the case of a radar homing seeker. However, range and range rate are not accurately known in a system using an infrared seeker.

guidance law as configuration A. A detailed diagram of the filter is shown in Fig. A.6-3; it estimates the three state variables y_d, $\dot{y}_d$ and a_t, assuming that both range (r_{tm}) and missile acceleration* (a_ℓ) are known. These estimates of y_d and $\dot{y}_d$ are combined to yield an estimate of $\dot{\hat{\theta}}$ according to

$$\dot{\hat{\theta}} = \frac{\dot{\hat{y}}_d}{r_{tm}} + \frac{v_c \hat{y}_d}{r_{tm}^2} \qquad (2.2\text{-}1)$$

The switches S_1 and S_2 (Fig. 2.1-2) are both in position 2 and Fig. 2.2-2 illustrates the mechanization of the guidance law. The Kalman filter is inherently a digital processor; therefore the acceleration command is computed discretely, rather than continuously. Observe that the estimate of target acceleration is not used for control in configuration B.

Guidance Laws C, D and E are all represented by the diagram in Fig. 2.2-3. In configurations C and D, the control laws are chosen to minimize the performance index

$$J = \lim_{\gamma \to 0} E \left\{ (\text{miss distance})^2 + \gamma \int_0^{t_f} a_c^2 (t)\, dt \right\} \qquad (2.2\text{-}2)$$

making use of known results from optimal stochastic control theory. Configuration C minimizes J, neglecting autopilot dynamics, resulting in $c_4 = 0$, $n' =$ constant, and c_3 is determined as a function of target bandwidth (λ_t) and time-to-go until intercept (t_{go}). Configuration D is derived including a first-order model of autopilot dynamics having bandwidth λ_m; for this case c_3 is the same as in law B, whereas n' and c_4 are both functions

*See footnote on page 2-7

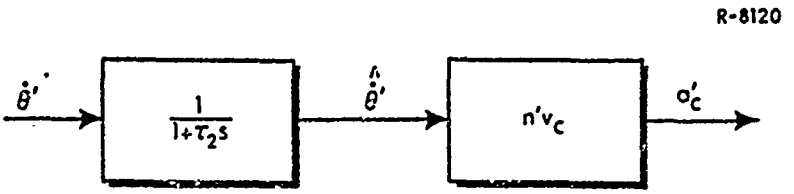

Figure 2.2-1 Guidance Law A

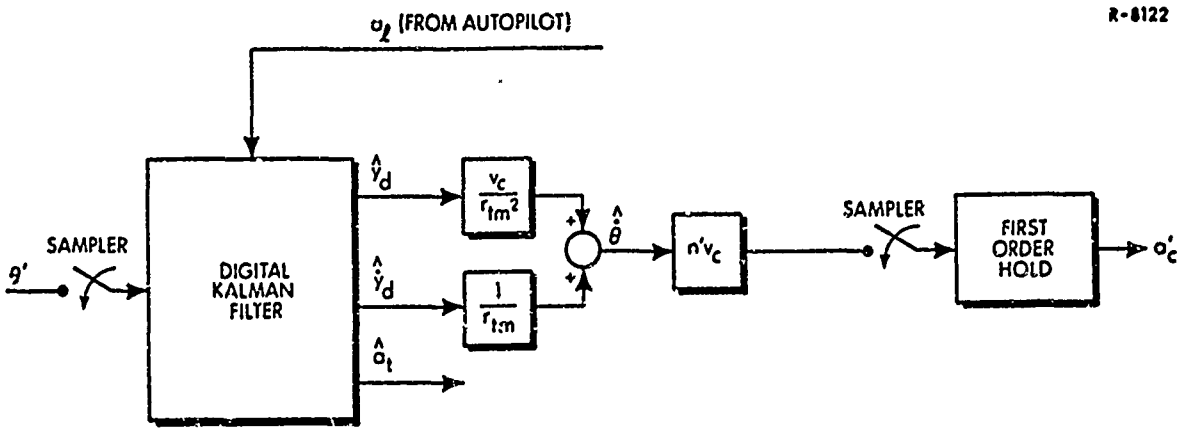

Figure 2.2-2 Guidance Law B

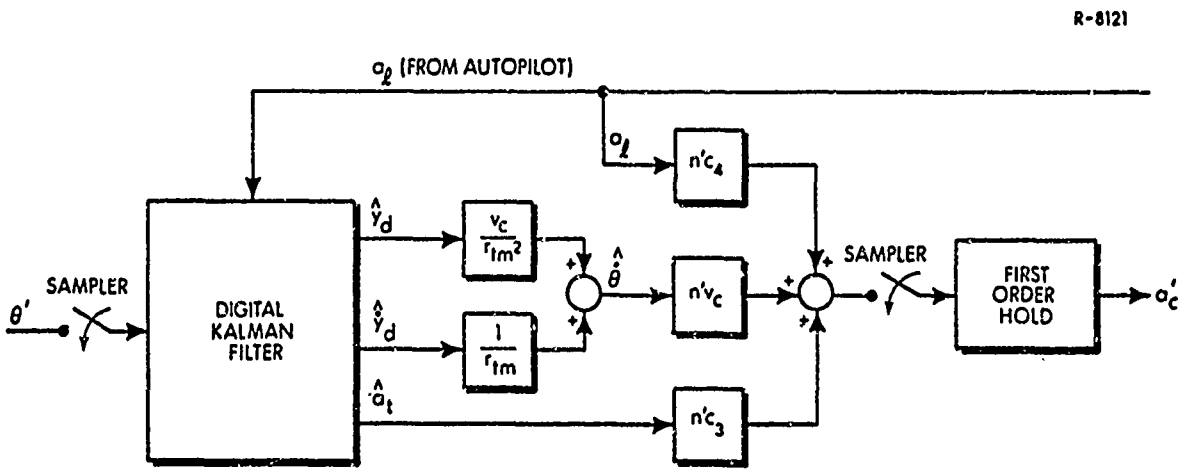

Figure 2.2-3 Guidance Laws C, D, and E

of λ_m and t_{go}. Both laws C and D are optimal linear guidance laws; the principal difference between them is that in law D, n' increases with decreasing range and becomes very large near intercept to compensate for the effective lag in missile acceleration caused by the dynamics of the missile-autopilot combination.

Configuration E is designed to minimize

$$J = E\left\{|\text{miss distance}|\right\} \tag{2.2-3}$$

subject to the explicit constraint

$$|a_c| \leq a_{max} \tag{2.2-4}$$

Because the limit on missile acceleration is accounted for in the problem formulation, the resulting optimal nonlinear guidance law differs from those described previously. The mechanization takes the same form as that in Fig. 2.2-3; the only difference is the manner in which n' is computed. Typically, the value of n' is much larger than for guidance law D over most of the trajectory, as indicated in Fig. A.6-4. This is explained by the fact that between seeker measurements, guidance law E attempts to completely null the predicted miss distance before the next seeker measurement is processed. By contrast, the other guidance laws effectively only attempt to reduce the predicted miss distance at each stage. This law is useful in the sense that it provides a lower bound on the miss distance that can be achieved, for the assumed airframe, seeker noise, etc.

The computational requirements of guidance laws B, C, D, and E are primarily dictated by the Kalman filter. In Section A.7 the following conservative estimates of storage capacity and processing time per measurement cycle are obtained for a typical existing digital minicomputer:

Storage ≅ 600 words

Processing Time ≅ 0.01 sec

The storage requirement is well within the memory capacity of modern lightweight computers, and the processing time is sufficiently small to achieve good missile control. Therefore, these guidance laws are judged to be potentially suitable for mechanization in tactical missiles, provided their performance is sufficiently superior to conventional laws to justify the cost of the computer. The issue of performance is treated in Chapter 3.

3. GUIDANCE SYSTEM EVALUATION

3.1 EVALUATION PROCEDURE

The Covariance Analysis Describing Function Technique (CADET) is a powerful new approximate method for analyzing the statistical behavior of nonlinear stochastic systems, particularly for developing performance sensitivity curves (Ref. 6). Its advantage lies in the fact that mean square values of system state variables for a given system design can be determined from one solution of a matrix differential (or difference) equation. By contrast, many solutions of the system equations of motion are required to analyze statistics by monte carlo techniques.

The guidance system model displayed in Fig. 2.1-2 has a mixed continuous-discrete character in the sense that the optimal guidance laws discussed in Chapter 2 process data at discrete times whereas the seeker, missile, and airframe equations of motion are described by differential equations. Appendix B presents a detailed explanation of how CADET is used to analyze such a system; the principal steps to be followed are summarized below:

- Replace each nonlinear element by its corresponding random input describing function gain, based upon an assumed probability density function for the input to the nonlinearity.
- Using the resulting linear system model, employ conventional covariance analysis techniques to propagate the statistics of the system state vector--i.e., its mean and covariance--recognizing that the describing function gains are functions of those statistics.

- Compute the rms miss distance at the intercept time from the elements of the system covariance matrix.

Typically, the input to each nonlinearity is a state variable that is assumed to be a gaussian random process. The gaussian assumption is based upon the fact that the system state variables tend to be a superposition of past values of both the nonlinearity outputs and various random system inputs. Thus, in the sense of the "central limit theorem" (Ref. 8), the probability density function for the system state variables tends toward the gaussian form, regardless of the densities of individual random events. Of course, this assertion is only approximately valid; the extent to which it holds depends upon the amount of low pass filtering in the system, the number of nonlinearities, and the bandwidth of the random inputs. To avoid actually calculating the required probability density function, a task at least as time-consuming as performing monte carlo simulations, the gaussian assumption stated above is imposed at the outset. Its validity for a specific system is investigated through comparisons with selected monte carlo results.

The two nonlinearities associated with the guidance system investigated in this study are the saturation and sine functions shown in Fig. 2.1-2. The corresponding describing function gains are computed as functions of their input statistics in Section B.5.

In all the cases treated here, the mean value of the system state vector is zero; hence we are concerned only with the propagation of the system covariance matrix according to the procedure described in Section B.4, and calculating the rms miss distance. The latter is given by the rms value of y_d (Fig. 2.1-3) at the intercept time. The next section gives comparisons of guidance law performance for a range of representative system parameter values.

3.2 SIMULATION RESULTS

In order to compare the performance of the guidance laws listed in Table 2.2-1, nominal values were chosen for the missile-target engagement initial conditions, and for the parameters of the model in Fig. 2.1-2. These quantities are listed in Table 3.2-1. All exceptions to the nominal conditions are explicitly stated in the subsequent discussion.

Observe that the autopilot parameters are chosen to yield first-order dynamics with a 0.1 sec time constant (10 sec^{-1} bandwidth). The seeker noise levels selected represent an angular measurement error of about 0.7 mrad at a missile-target separation of 10,000 feet. The missile-target initial conditions yield a nearly head-on intercept trajectory.

To determine the validity of CADET as an analysis technique, the rms miss distance was computed using both monte carlo and CADET techniques for selected trajectories. Results are shown in Fig. 3.2-1 for conventional proportional guidance (Law A), as a function of the missile acceleration limit; other off-nominal conditions are stated in the figure. The monte carlo points are obtained from 200 missile trajectory simulations. The dashed line represents the value of rms miss which would be obtained from a linear covariance analysis that neglects all the nonlinear effects.

Evidently, the discrepancy between CADET and monte carlo results tends to increase as a_{max} decreases. This is to be expected because the system nonlinear behavior becomes more pronounced as a_{max} decreases and CADET, being an approximate method for analyzing nonlinear systems, will tend to have larger errors. However, the fact

TABLE 3.2-1

NOMINAL CONDITIONS

Quantity	Nominal Value Specification
Autopilot Parameters a_1	0
Autopilot Parameters a_2	0
Autopilot Parameters b_1	0.1 sec
Autopilot Parameters b_2	0
Autopilot Parameters b_3	0
Target Maneuver Bandwidth, λ_t	0.2 sec^{-1}
rms Target Acceleration, σ_t	300 ft/sec^2
Missile Acceleration Limit, a_{max}	800 ft/sec^2
Seeker Time Constant, τ_1	0.1 sec
Radome Slope Parameter, k_r	0
Guidance Navigation Ratio (Laws A, B, and C only), n'	3
Launch Range	24,000 ft
rms Heading Error	0.15 rad
Closing Velocity (assumed constant)	4000 ft/sec
Target Velocity	1000 ft/sec
Interceptor Velocity	3000 ft/sec
Noise Parameters: Receiver, σ_r/r	4×10^{-8} ft^{-1}
Noise Parameters: Scintillation, $\sigma_s r$	4 ft
Noise Parameters: Range Independent, σ	4×10^{-4} rad

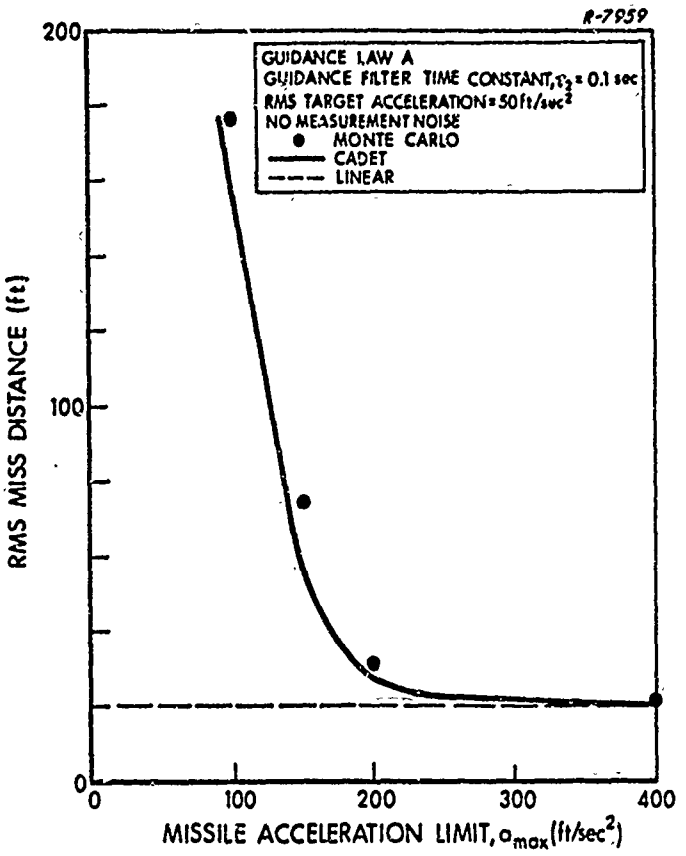

Figure 3.2-1 Cadet-Monte Carlo Comparison versus Missile Acceleration Capability

that CADET captures the major effect of the nonlinearity, and gives accurate results when the system is moderately nonlinear--e.g., when a_{max} = 200 ft/sec^2 in Fig. 3.2-1--makes it a valuable technique for comparing different guidance system designs.

The justification for using CADET lies in the time saving realized relative to the monte carlo approach. The monte carlo points in Fig. 3.2-1 each required 720 seconds of computer time; the corresponding values from the CADET results each require 25 seconds of computer

time. Thus many more parameter studies of a nonlinear guidance system can be achieved with CADET, for a given computational budget.

All five guidance laws are compared in Fig. 3.2-2 over a range of values for the target maneuver bandwidth.* In order that Law A (proportional guidance) be fairly compared with the others, its filter time constant, τ_2 in Fig. 2.2-1, is optimized to yield the lowest value of rms miss distance for each value of λ_t. The dispersion between the various laws generally increases with λ_t. However, the major improvement over conventional proportional guidance is achieved through use of Law C, which adds a control gain to account for target maneuvers. Some additional improvement is achieved by accounting for missile autopilot dynamics (Law D). Guidance law E provides a lower bound on the achievable miss distance, neglecting the effect of the kinematic sine-function nonlinearities in Fig. 2.1-2. (The latter are included in the truth model but not in the design model.)

Observe that there is no appreciable difference between the performance of Laws A and B, although Law B should be superior because it employs a Kalman filter to estimate line-of-sight rate. This is explained by the fact that most of the miss distance associated with proportional guidance law is caused by target maneuvers, rather than homing sensor measurement noise. This is illustrated in Fig. 3.2-3 for a case with no target maneuver and larger noise levels. Evidently the miss distance achieved with the Kalman filter is about half that achieved with an optimized first-order filter. However, this difference is not

*Guidance Laws B through D listed in Table 2.2-1 depend upon knowledge of the bandwidths of the target maneuver (λ_t) and the first-order design model for the autopilot (λ_m). Unless otherwise stated in the following discussion, it is assumed that these quantities are equal to the values assumed for the truth model; i.e., the optimal guidance laws are matched to the truth model.

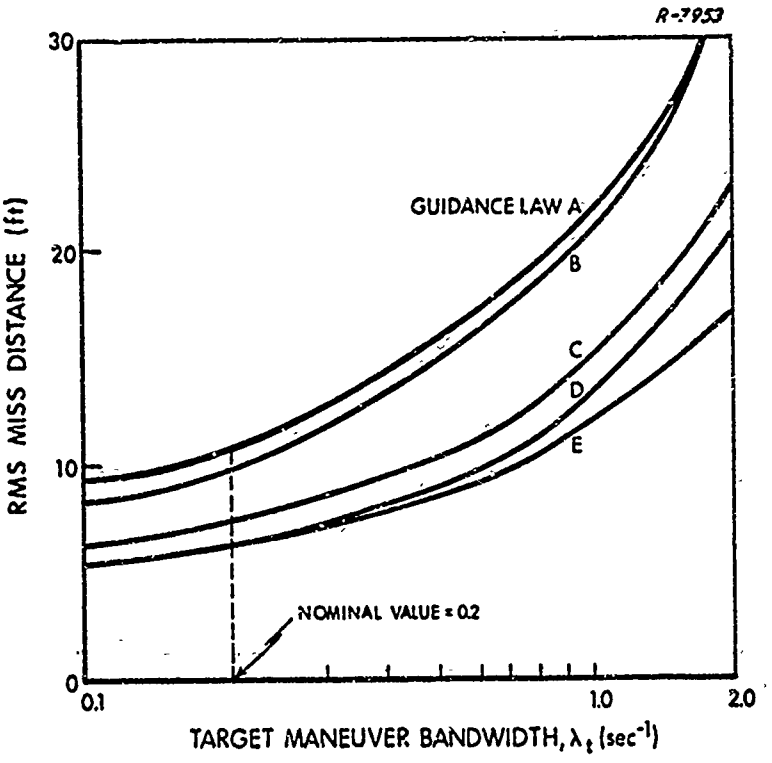

Figure 3.2-2 Guidance Law Performance versus Target Maneuver Bandwidth

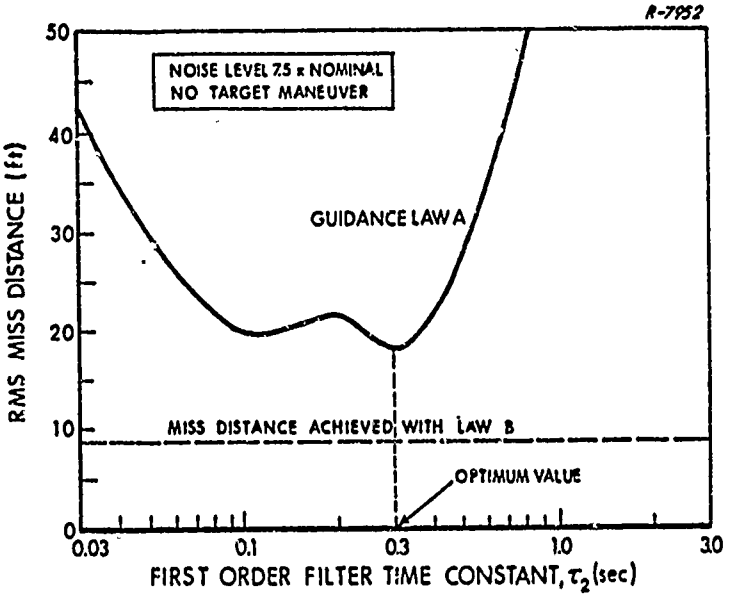

Figure 3.2-3 Performance of Proportional Guidance Using a Kalman Filter versus a First-Order Filter

significant at the nominal noise levels, when target maneuvers are also present.

Another aspect of the comparison in Fig. 3.2-2 is the fact that Laws A, B and C have constant navigation ratios, whereas those associated with D and E are time-varying. The performance of the first three laws can be improved if their associated values of n' are optimized, in the same fashion as the filter time constant associated with Law A is optimized in Fig. 3.2-3. This is demonstrated in Fig. 3.2-4 for Law B. Generally, n' should be larger than the value three, which is obtained in Section A.6, assuming no target acceleration and neglecting autopilot dynamics, to compensate for target maneuvers and autopilot dynamics.

Figure 3.2-5 displays guidance law performance as a function of missile maneuver capability*. As a_{max} approaches the target rms acceleration level (300 ft/sec^2), Laws C, D, and E offer marked improvement over proportional guidance (Law B). In addition, the dispersion between D and E increases; this is attributable to the fact that Law E explicitly accounts for the acceleration limit whereas D does not. Hence the former offers greater improvement over the latter as acceleration saturation becomes more pronounced; this effect is also observed in Ref. 7.

The influence of the missile autopilot time constant on miss distance is demonstrated in Fig. 3.2-6. As the latter gets larger, Laws D and E, which explicitly account for autopilot dynamics, offer significantly better performance than Laws B and C. This is primarily

*Law A is omitted from this and further guidance law comparisons on the basis that it yields performance quite close to Law B when its filter time constant is optimized (see Fig. 3.2-2) at the nominal noise levels.

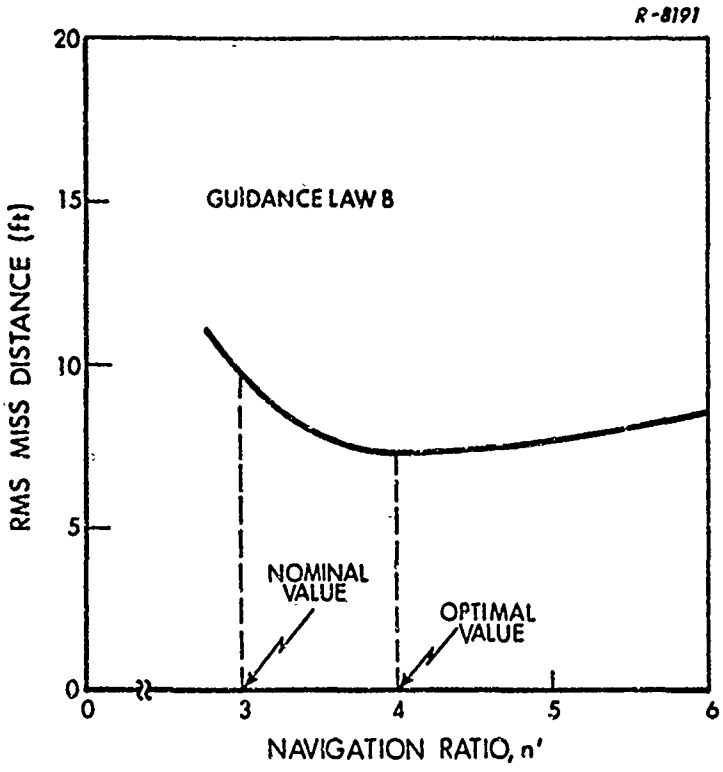

Figure 3.2-4 Performance of Proportional Guidance as a Function of the Navigation Ratio

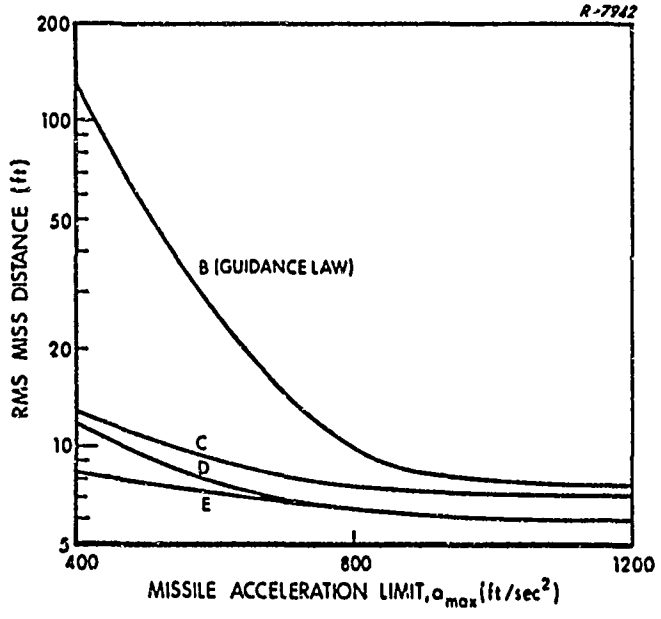

Figure 3.2-5 Guidance Law Performance versus Missile Maneuver Capability

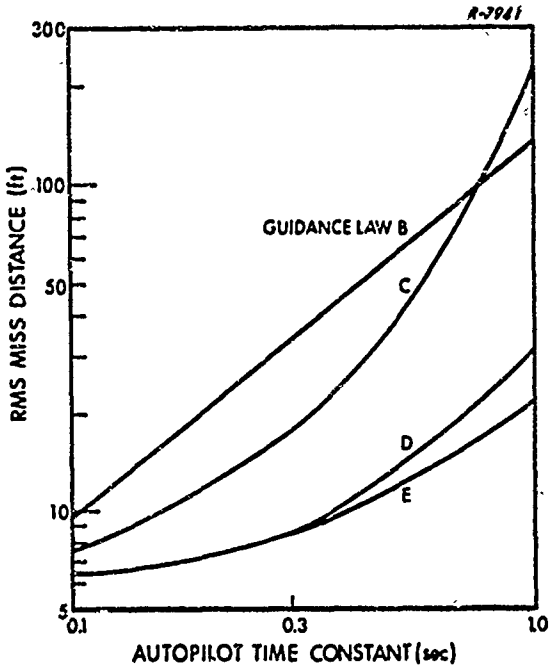

Figure 3.2-6 Guidance Law Performance versus Missile Autopilot Time Constant

attributed to the large values of n′ (see Fig. A.6-4) used in Laws D and E over portions of the missile trajectory.

Figure 3.2-7 compares the performance of Laws B, D, and E as a function of target acceleration. Ordinarily one might expect the miss distance to increase more rapidly with target acceleration than these curves indicate. This is explained by the fact that the target trajectory turns, while evading the missile, so that the component of its lateral acceleration normal to the line-of-sight is reduced. The greater the target acceleration, the more its trajectory turns and the greater the reduction in its effective maneuvering acceleration, normal to the LOS. In the limit when the target's acceleration becomes directed along the line-of-sight, it will have little influence upon miss distance. Thus, the curves in Fig. 3.2-7 tend to level off at large maneuver levels. This behavior is captured by the kinematic sine-functions nonlinearities shown in Fig. 2.1-2; it would not be visible in a purely linear system analysis.

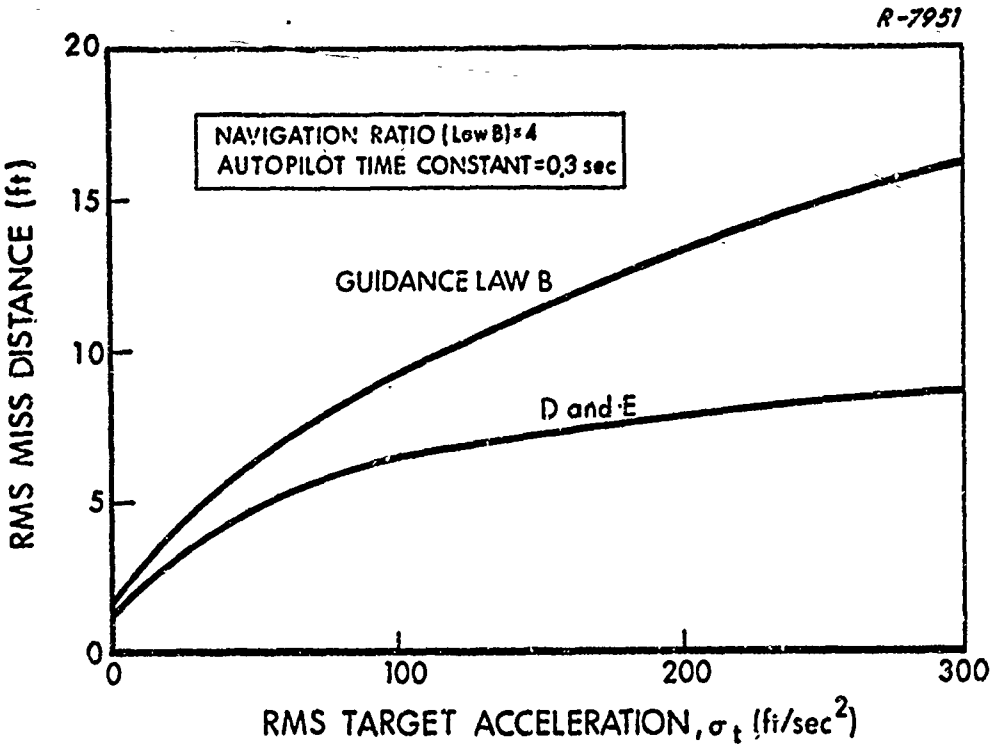

Figure 3.2-7 Guidance Law Performance versus Target Maneuver Level

In all the cases treated thus far, the design of guidance Laws D and E is matched to the truth model representation of missile dynamics, except for the kinematic nonlinearities mentioned above. An important issue remaining to be investigated is the sensitivity of guidance law performance to variations in missile parameters from their assumed values.

Recall that one of the potentially important effects is autopilot-seeker coupling through the seeker aberration effect. This is represented in Fig. 2.1-2 by the constant k_r, which has heretofore been chosen as zero. Figure 3.2-8 illustrates the effect on guidance system performance

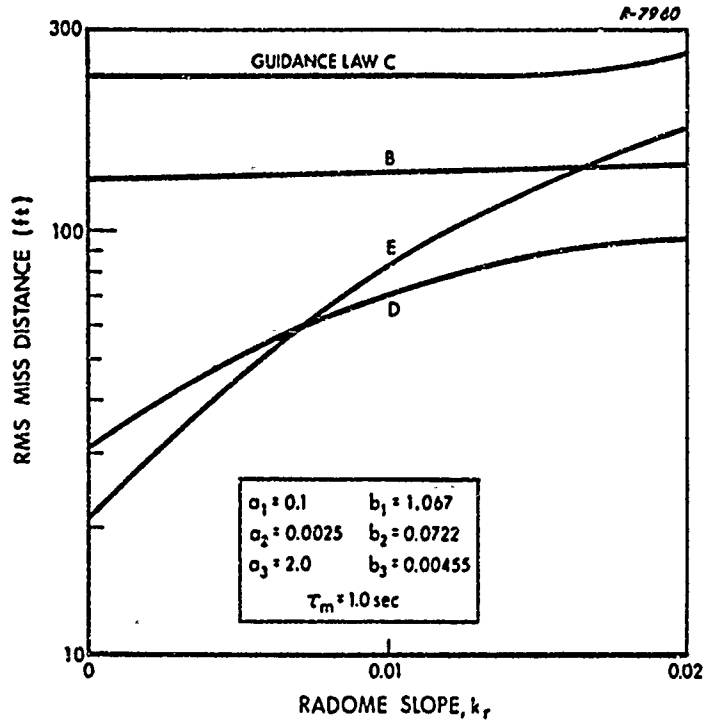

Figure 3.2-8 Guidance Law Sensitivity to Aberration Error; Dominant Autopilot Pole =-1.0 sec^{-1}

when k_r is nonzero. For this case, the parameters a_1, a_2, b_1, b_2, and b_3 are selected to yield autopilot poles at -1 rad/sec and -7.5 ±j15 rad/sec, and zeros at ± 20 rad/sec. The design model for Laws D and E assumes the autopilot is first-order with time constant (τ_m) equal to 1 sec. The value of a_3 is chosen to be representative of high altitudes, where autopilot seeker coupling is most pronounced. With the exception that here $k_r \neq 0$, the above conditions are nearly the same as those in Fig. 3.2-6 when the autopilot time constant = 1.0 sec. Figure 3.2-9 displays the sensitivity to k_r for another case where the dominant autopilot pole is 3.3 rad/sec.

As k_r increases, the performance advantage of Laws D and E deteriorates relative to Laws B and C. This is attributed to the fact that the high value of n' associated with Laws D and E is incompatible with

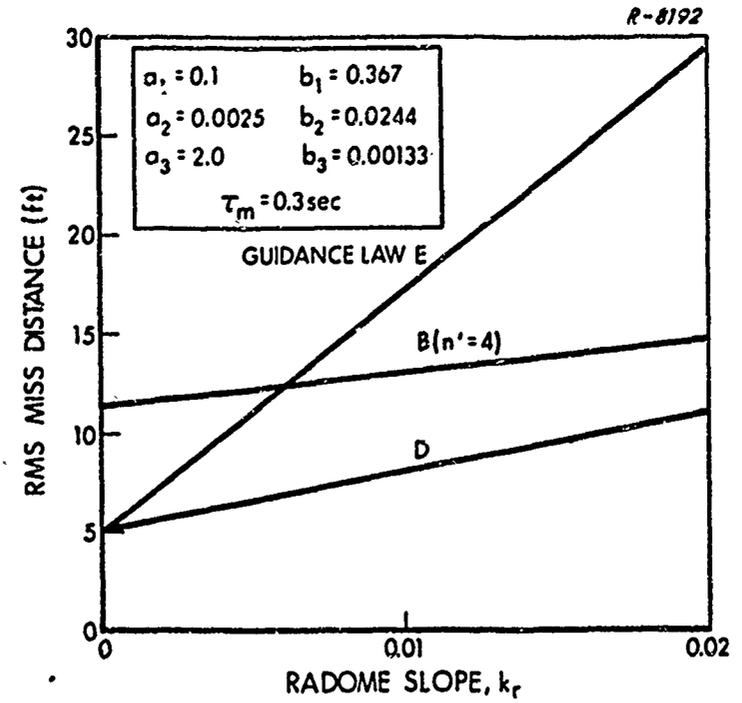

Figure 3.2-9 Guidance Law Sensitivity to Aberration Error ; Dominant Autopilot Pole = -3.3 rad/sec

the parasitic attitude loop in Fig. 2.1-2, because the latter is not accounted for in the derivation of the guidance law. Generally k_r may be an unknown, even time-varying quantity, so that it cannot be accounted for exactly. Consequently, some degradation in the performance of the "high-gain" guidance laws will be experienced in situations where the effect of k_r is important--i.e., at high altitudes. The performance of Law E tends to degrade more rapidly than the other guidance laws because of its relatively large navigation ratio (see Fig. A.6-4). It is the most sensitive to errors in the design assumptions.

Finally, the sensitivity of guidance law performance to an error in knowledge of the dominant autopilot time constant is shown in Fig.

3.2-10 for Laws D and E. The actual time constant is 1 sec, corresponding to the conditions at the right hand side of the graph in Fig. 3.2-6; the design value of the autopilot time constant (τ_m) is varied over the range indicated on the abscissa in Fig. 3.2-10. When the design value of τ_m is one, both laws E and D are matched to the autopilot and law E has the best performance. When $\tau_m \neq 1$, Law E degrades more rapidly than Law D because of its larger navigation ratio.

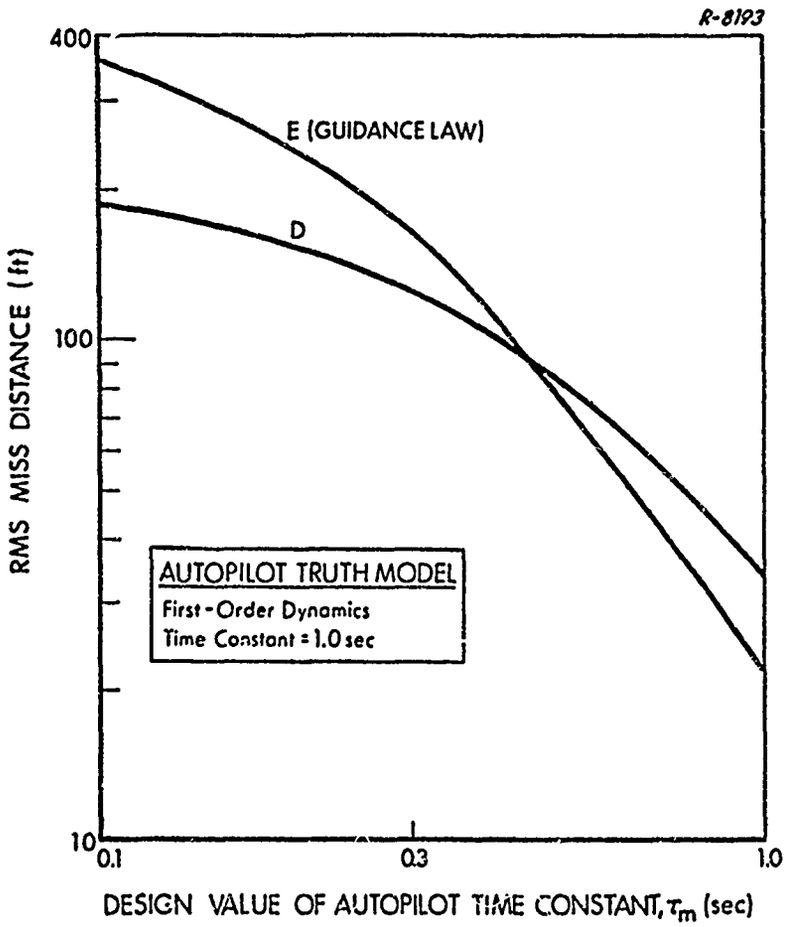

Figure 3.2-10 Guidance Law Sensitivity to Design Value of the Autopilot Time Constant

4. SUMMARY AND CONCLUSIONS

4.1 SUMMARY

This report presents comparisons of performance for the guidance laws summarized in Table 4.1-1 and derived in Appendix A. Each law is evaluated in a guidance system model that incorporates significant linear and nonlinear dynamic effects. These include the following missile characteristics: homing seeker noise, homing seeker dynamics, autopilot dynamics, maneuvering acceleration limit, parasitic autopilot-seeker dynamic coupling, random target accelerations, and nonlinear missile-target geometric effects. The rms miss distance achieved with each guidance law is calculated using a recently developed analytical procedure for determining the statistical properties of nonlinear systems--the Covariance Analysis Describing Function Technique (CADET). The latter achieves a good approximation to monte carlo results, and offers the advantage of requiring significantly less computation time.

TABLE 4.1-1

MISSILE GUIDANCE LAWS

Guidance Laws	Distinguishing Characteristics	Type of Noise Filter
A	Proportional Guidance	First-Order, Low-Pass
B	Proportional Guidance	Kalman
C	Optimal Linear Guidance; Accounts for Target Maneuvers	Kalman
D	Optimal Linear Guidance; Accounts for Target Maneuvers and Missile Autopilot Dynamics	Kalman
E	Optimal Nonlinear Guidance; Accounts for Target Maneuvers Missile Autopilot Dynamics, and Missile Airframe Saturation	Kalman

4.2 CONCLUSIONS

The principal conclusions of this work are as follows:

- Conventional proportional guidance using a first order filter (Law A) is adequate for nonmaneuvering targets and moderate homing sensor noise levels. The miss caused by large noise levels can be reduced by as much as 50 percent using a Kalman filter (Law B) to process seeker measurements.
- Guidance Law C generally offers the biggest relative improvement over proportional guidance against maneuvering targets, provided the missile autopilot time constant is small (< 0.2 sec).
- Guidance Laws D and E are significantly better than Law C when the missile autopilot time constant is large (> 0.2 sec).
- Laws D and E are sensitive to errors in the design assumptions about the missile autopilot dynamics; Law E is most sensitive because of its relatively large control gains.
- The principal computational burden imposed by the optimal guidance laws is associated with the Kalman filter. The storage capacity and measurement processing time needed to mechanize the filters are conservatively estimated at 600 words and 0.01 sec, respectively. These requirements are compatible with modern airborne-type computers.
- CADET is found to be a useful technique in analyzing guidance system performance. The saving in computer time over 200 run monte carlo analysis is about 30:1 for the system model used in these studies.

The above conclusions, together with the quantitative performance results provided in Chapter 3 will provide a basis for choosing among optimal guidance laws in particular applications.

APPENDIX A

TRUTH MODEL DEVELOPMENT

A meaningful comparison of homing guidance systems for tactical missiles requires realistic models for the missile and its target engagement geometry model in order to accurately evaluate terminal miss distance. This model should include the important dynamics and system nonlinearities which influence performance, and yet be representative of tactical missiles in general. A system truth model that satisfies these requirements is developed in this appendix. The various modules discussed in subsequent sections are based on the functional diagram in Fig. 2.1-1. It should be noted at the outset that the model developed herein assumes that the target and missile motion are constrained to a plane. Consequently, development of the missile and guidance models is limited to a single channel.

A.1 SEEKER MODULE

The function of the seeker subsystem is two-fold; it provides the measurements of target motion required to mechanize the guidance law, and it tracks the target with the antenna or energy receiving device.* The typical seeker hardware consists of two or three gimbals on which are mounted gyros and an antenna. Associated with each gimbal is a servomechanism which is used to adjust its angular orientation in response to the tracking error signal measured by the radar receiver. (Only one gimbal and its associated dynamics is required for the planar motion model.) It should be noted that there are also body mounted antenna systems which do not use moveable gimbals to position the antenna. These systems use either a fixed antenna position relative to the missile or electronic beam steering by means of a phased array (radar) antenna. These configurations are rather atypical of tactical missiles and will not be specifically considered, although the use of electronic

*Generally we shall use the term "antenna" to refer to any type of energy collecting device--radar, infrared, or optical.

beam steering is in many ways analogous to the gimballed system as far as the resulting guidance system operation is concerned.

Seeker Measurement Geometry – The fundamental measurement obtained from the homing sensor receiver is assumed to be the indicated angular position of the target relative to the antenna center-line or boresight. The guidance laws considered in this report require line-of-sight (LOS) angle or LOS angular rate as the fundamental measurement for terminal guidance. Illustrated in Fig. A.1-1, the LOS angle, θ, is the angle between a line from the center of the seeker antenna to the target, and some arbitrary non-rotating reference line. It is convenient to select this reference equal to the LOS position at the beginning of the homing guidance phase. Consequently, $\theta(t)$ at time t is the total change in the angular position of the LOS relative to the initial LOS.

The angular position of the missile body center line, θ_m, is measured relative to the initial LOS as shown in Figure A.1-1. The angular position of the antenna centerline measured relative to the body centerline is defined as θ_h in Figure A.1-1. Therefore, θ is given by

$$\theta = \theta_m + \theta_h + \epsilon \qquad \text{(A.1-1)}$$

Alternatively, by writing Eq. (A.1-1) as

$$\epsilon = \theta - \theta_m - \theta_h \qquad \text{(A.1-2)}$$

we obtain an expression for the true boresight error. It is important to note that boresight error is a function of both the missile attitude relative to inertial space and the angular position of the antenna relative to the missile center-line. Since θ or $\dot{\theta}$ is the desired measurement for guidance purposes, it is necessary to remove missile motion from the LOS measurement data.

R-7153a

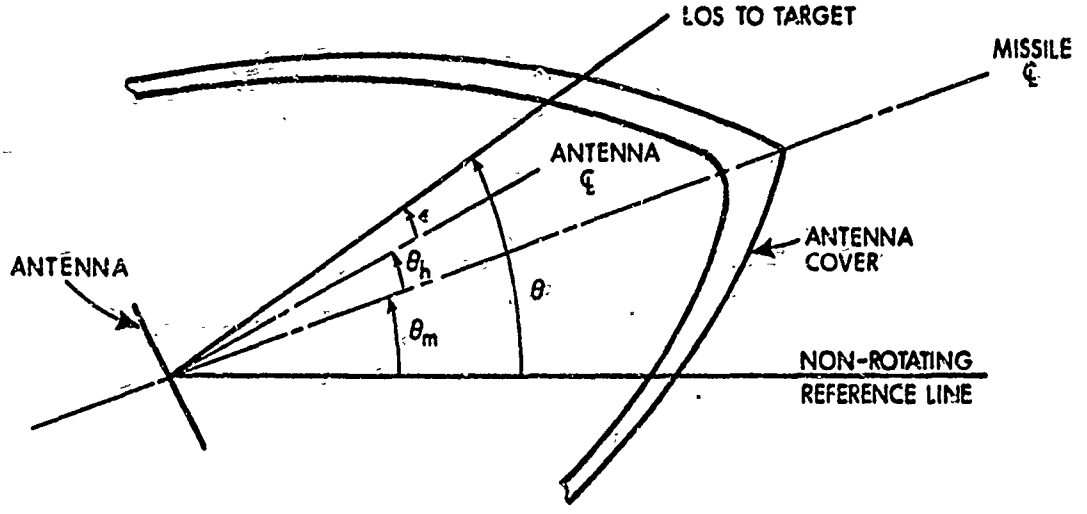

Figure A.1-1 Seeker-Radome Geometry

One requirement on the seeker system is to keep the antenna pointed at the target so that ϵ is always much smaller than the beam width of the received energy. In the region of small ϵ, the seeker receiver measurement of indicated boresight error is nearly linear. However, if ϵ cannot be considered small relative to the antenna beamwidth, the receiver boresight error processor operation may become nonlinear, as illustrated in Fig. A.1-2. In fact, if ϵ is allowed to approach the half beamwidth of the antenna, the receiver detection circuitry will at some point loose lock and all guidance information will be lost. Therefore, the seeker must track the target sufficiently closely so that large boresight errors do not occur. Otherwise the nonlinearity of the boresight error position should be considered as an important system nonlinearity. Since the actual form of the boresight error processor nonlinearity is strongly dependent on the specific beam width, processing scheme (monopulse radar, c.w. radar, etc.) and detector characteristics of individual systems, it will not be included in the general system model for the current study. It will be assumed that the beam width and the tracking

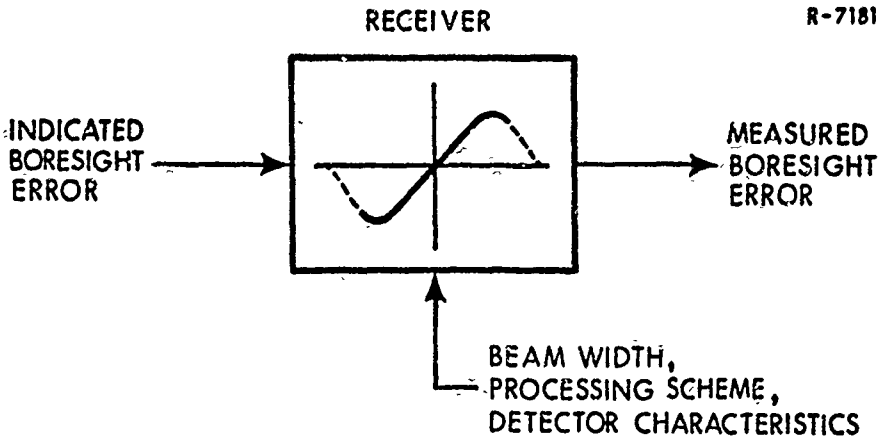

Figure A.1-2 Signal Processing Nonlinearities

response of the seeker are adequate to keep the boresight error processor in its linear region.

Aberration Error – The aberration angle error is the result of nonlinear distortions in the received energy as it passes through the protective covering (radome in the case of a radar homing sensor) over the antenna. This distortion produces a false boresight error signal, ϵ', which is interpreted as an error in the angular position and motion of the target by the guidance package. Referring to Fig. A.1-3, the indicated boresight error in the presence of aberration angle, θ_r, is given by by

$$\epsilon' = \theta + \theta_r - \theta_m - \theta_h \qquad \text{(A.1-3)}$$

The size of this measurement error, θ_r, depends on the orientation of the antenna with respect to the antenna cover, which is fixed to the missile airframe. This dependency of θ_r on θ_m couples body motion into the boresight error signal, thus forming what is called the "parasitic attitude loop". The latter can drastically alter missile response characteristics and in turn increase miss distance. This is particularly true at high altitudes where the missile body motion tends to be greatest. (This effect is discussed more fully in Section A.3).

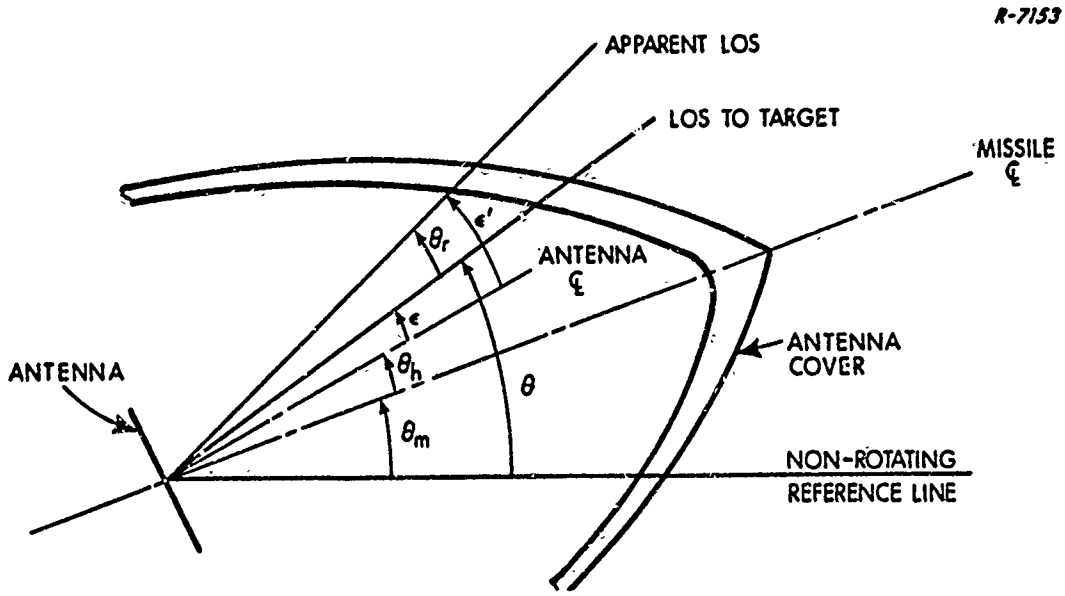

Figure A.1-3 Effect of Aberration Error

The aberration angle error can be a nonlinear function of several factors: the angle between the missile center line and the LOS to the target (look angle) as illustrated in Fig. A.1-4; the thickness distribution, material, shape, and optical or electrical properties of the antenna cover; frequency, and polarization of the received signal; manufacturing tolerances; erosion of the surface during flight. Therefore, an accurate model may require a nonlinear, time-varying statistical characterization of the radome. However, since these characteristics tend to vary over rather wide limits depending on the particular application and missile configuration, a constant aberration error slope model is used to capture the important body coupling effect, consistent with the desire for a general system model.

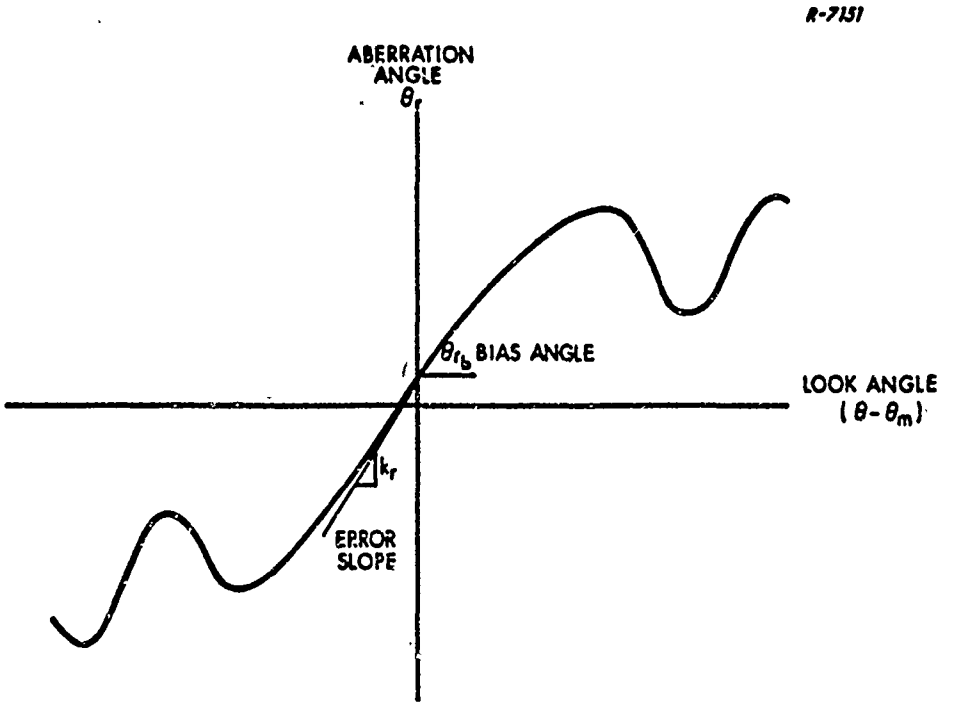

Figure A.1-4 Typical Aberration Angle Error as a Function of Look Angle

A linear model for the general aberration angle characteristic given in Fig. A.1-4 is obtained from a simple Taylor series approximation

$$\theta_r = \theta_{rb} + (\theta - \theta_m)\, k_r \qquad (A.1\text{-}4)$$

where k_r is the error slope and θ_{rb} is a bias angle. Substituting Eq. (A.1-4) into Eq. (A.1-3) for ϵ' yields

$$\epsilon' \cong (1 + k_r)(\theta - \theta_m) + \theta_{rb} - \theta_h \qquad (A.1\text{-}5)$$

The boresight error bias will be assumed negligible relative to other system errors. There also is a possible contribution of the aberration error to measurement noise when the frequency of the received signal is varied in

a pseudo-random fashion to reduce the effect of a potential enemy jammer, e.g., when the seeker is an active or semiactive radar. This noise is simply treated as a contributor to range independent noise (Section A.2).

Seeker Track and Stabilization Loops – The assumed configuration for the seeker is illustrated in Fig. A.1-5. The indicated boresight error, ϵ', is scaled by $1/\tau_1$, which forms the desired rate command to the stabilization loop. (Although an actual system requires the implementation of two or three channels to account for motion in three dimensions, only one channel is required for the planar intercept model considered herein.)

R-9210

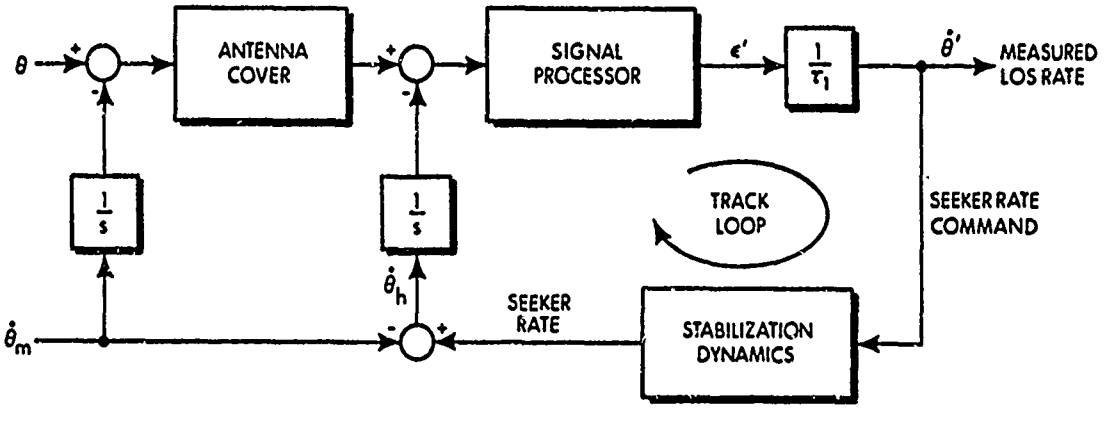

θ = Line-of-sight angle
ϵ' = Measured boresight error angle
$\dot{\theta}_h$ = Seeker gimbal angle rate relative to missile
$\dot{\theta}_m$ = Missile attitude angle rate
τ_1 = Track loop time constant

Figure A.1-5 Seeker Subsystem Block Diagram

The stabilization dynamics are comprised of the gimbal servo and rate gyro (mounted on the antenna) and typically have very wide bandwidth; e.g., greater than 100 rad/sec. The track loop model has simple first-order dynamics; it commands a gimbal rate proportional to the measured boresight error. The loop attempts to drive the boresight error to zero, thereby causing the antenna to track the target. It is straightforward to show that the linear transfer function from $\dot{\theta}$ to ϵ' -- assuming unity gain for the antenna cover, the signal processor, and the stabilization dynamics -- is

$$\frac{\epsilon'}{\dot{\theta}} = \frac{\tau_1}{1 + s\tau_1} \qquad \text{(A.1-6)}$$

Therefore, at low frequencies ($\omega < 1/\tau_1$), the indicated boresight error is proportional to the LOS rate. The latter is the desired measurement for classical proportional navigation guidance, which commands a missile lateral acceleration proportional to the LOS rate.

It was assumed in the above development of the seeker operation that the boresight error processor nonlinearity illustrated in Fig. A.1-2 could be neglected. Equation (A.1-6) provides an indication of the important region of boresight error linearity. Using the fact that ϵ' is proportional to $\dot{\theta}$ in steady state for a constant $\dot{\theta}$, we obtain the following expression for ϵ'_{max}:

$$\epsilon'_{max} = \tau_1 \dot{\theta}_{max} \qquad \text{(A.1-7)}$$

If τ_1 is sufficiently small, ϵ'_{max} can be held within the linear range of the received beamwidth. The resulting seeker block diagram with the linear aberration error model is given in Fig. A.1-6.

The importance of the aberration angle error slope, k_r, is illustrated by the linear, continuous transfer function relating θ_m to θ' in Fig. A.1-6. The latter is given by

$$\frac{\theta'}{\theta_m} \cong \frac{-k_r}{(1+\tau_1 s)} \qquad \text{(A.1-8)}$$

Thus the measured LOS rate is corrupted by a term proportional to body rate. Since body rate is a result of commanded acceleration, a loop is formed which can have a destabilizing effect on missile attitude and increase miss distance. Note that when k_r is zero, the contributions from the body angular rate input in Fig. A.1-6 cancel, producing no effect on ϵ'.

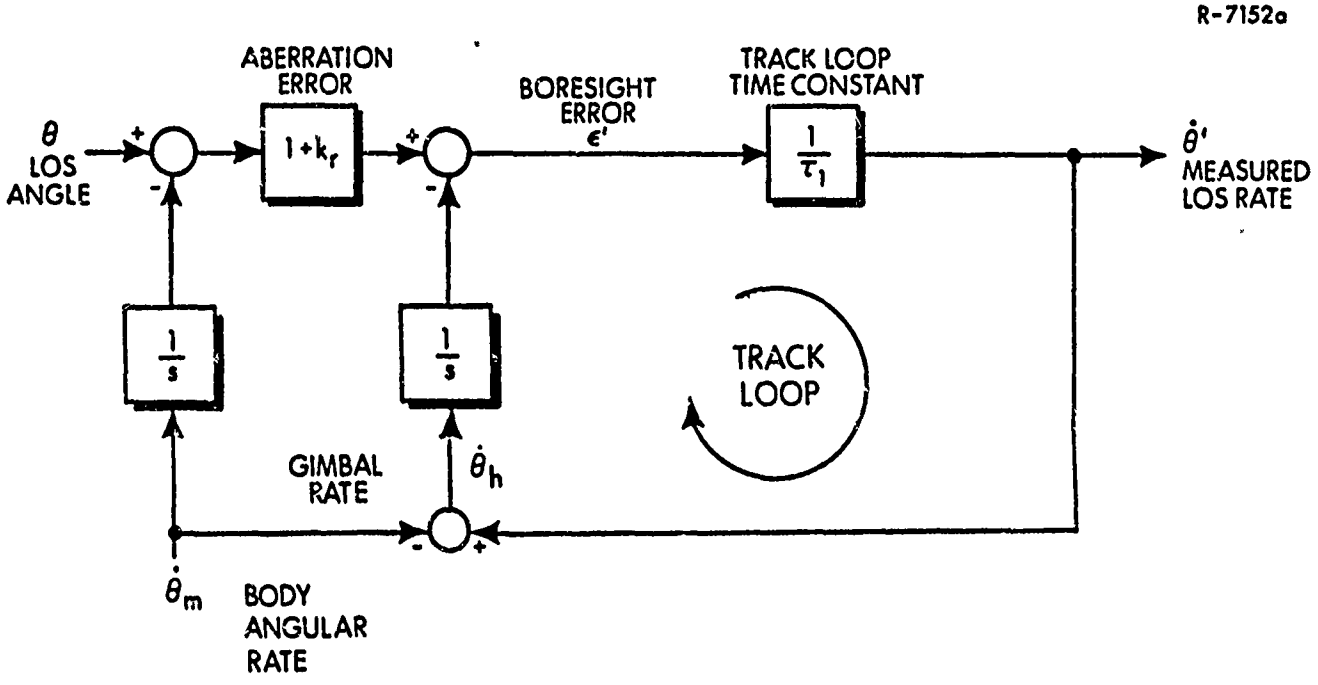

Figure A.1-6 Seeker Model with Track Loop

LOS Angle Measurement — Although classical proportional guidance uses measurements of LOS rate, it is more convenient to use measurements of LOS angle in guidance laws that utilize a Kalman filter. To obtain the latter, we define the measured LOS angle, θ', as

$$\theta' = (1+k_r)\,\theta - k_r\,\theta_m \qquad \text{(A.1-9)}$$

Then from Fig. A.1-6 it follows that

$$\epsilon' = \frac{\tau_1 s\,\theta'}{1+\tau_1 s} \qquad \text{(A.1-10)}$$

Since the boresight error is an observable quantity, Eq. (A.1-10) can be inverted to yield

$$\theta' = \frac{1+s\tau_1}{\tau_1 s}\,\epsilon' \qquad \text{(A.1-11)}$$

That is, θ' can be recovered from the measured seeker boresight error. This is represented in Fig. 2.1-2 by direct pickoff of θ'.

A.2 NOISE MODULE

As indicated in Section A.1, LOS angle is the fundamental quantity measured by the Seeker Module. These measurements will generally be corrupted by various types of noise which can be categorized according to the dependency of their rms levels on the missile-to-target range. The actual noise levels and bandwidths are dependent on the exact form of the measurement signal processor, target configuration

and characteristics, environmental conditions and a multitude of related system effects. However, using measurements obtained from actual hardware or mathematical models, most of the observed measurement noise can be lumped into one of three assumed forms: receiver* noise, range independent noise or angular scintillation noise.

Receiver Noise – Receiver noise consists primarily of thermal noise generated by the antenna and receiver electronics on board the missile. The effective amplitude of this noise increases with increasing range because of the corresponding decreasing signal-to-noise ratio. There are in general three types of missile receivers which can be considered:

- Passive – Target supplies radiated signal
- Semi-Active – Target is illuminated by a source which is not on board the missile
- Active – Target is illuminated by source on board the missile

The receiver will generally include some type of automatic gain control which attempts to keep the receiver signal power nearly constant. As a result, the effective noise level will change with received signal power relative to some reference level. A normalized angular measurement noise model will be defined which uses the variance (or power spectral density) of the indicated boresight error, measured at a range that yields a signal-to-noise ratio of unity as the reference level. The resulting expressions for the variances of the effective noise on the LOS angle for the three types of receivers are:

*Again, the term receiver can refer to any type of homing sensor.

Passive

$$\sigma_r^2 = \sigma_{rp}^2 \left(\frac{r_{tm}}{r_0} \right)^2 \qquad \text{(A.2-1)}$$

Semi-Active

$$\sigma_r^2 = \sigma_{rsa}^2 \left(\frac{r_{tm} r_{it}}{r_0^2} \right)^2 \frac{\sigma_0}{\sigma_t} \qquad \text{(A.2-2)}$$

Active

$$\sigma_r^2 = \sigma_{ra}^2 \left(\frac{r_{tm}}{r_0} \right)^4 \frac{\sigma_0}{\sigma_t} \qquad \text{(A.2-3)}$$

where:

r_{tm} = missile-to-target range

r_{it} = illuminator-to-target range

r_0 = range at which S/N = 1

σ_{rp}^2 = passive noise variance at S/N = 1

σ_{rsa}^2 = semi-active noise variance at S/N = 1

σ_{ra}^2 = active noise variance at S/N = 1

σ_t = effective target crossection

σ_0 = reference target crossection

All three types of receiver noise exhibit the characteristic of increasing variance with increasing range. Also, note that the passive model is not dependent on the effective target crossection since the energy received by the missile is direct radiation and not the result of reflected energy.

Often the illuminator to target range for a semi-active radar is nearly constant; in this case the semi-active noise variance will have nearly the same variation with r_{tm} as the passive noise for a given target crossection. Since most tactical missiles tend to be passive or semi-active, the passive noise model will be used in the truth model.

The noise bandwidth is dictated by the post-detection bandwidth of the receiver which in general tends to be much larger than the signal bandwidth. Consequently, it can be assumed that the noise is "white" over the signal spectrum of interest without loss of generality. In the case of a sampled data system, errors in the sampled and held values of LOS angle are assumed to be uncorrelated from sample to sample. If it is assumed that the receiver has a double-sided square spectrum Δ_f Hz in width with a constant noise power spectral density of q_r rad^2/Hz, the variance of the noise is simply

$$\sigma_r^2 = q_r \Delta_f \ (rad^2) \qquad \text{(A.2-4)}$$

If the receiver output is sampled and held with a sample period of τ_s sec, where τ_s is much larger than $1/\Delta_f$, resulting in independent noise samples, the output noise spectral density, q_s, has a low frequency level of approximately

$$q_s \cong q_r \Delta_f \tau_s = \sigma_r^2 \tau_s \quad \left(\frac{rad^2}{Hz}\right) \qquad \text{(A.2-5)}$$

Assuming that the bandwidth of the signal is smaller than the sampling frequency, Eq. (A.2-5) yields the level of the equivalent white noise spectral density.

Range Independent Noise – Range independent noise is a collection of all noise sources which contribute a constant rms error in the measurement of LOS angle throughout the flight. Typical sources include

servo noise generated by the seeker servo, and target amplitude scintillation noise. It will be assumed that the noise is also white over the receiver bandwidth, and the preceeding discussion of bandwidths and sampling is applicable. The variance of the range independent noise is defined as σ^2.

Angular Scintillation Noise - Angular scintillation noise is caused by the wandering of the apparent centroid of radiation across the visible surface of the target. Although the magnitude of the wander is essentially range independent, the equivalent noise on the LOS angle measurements increases as range decreases, resulting in a measurement noise variance of

$$\sigma_s^2 = \frac{\sigma_{wd}^2}{r_{tm}^2} \qquad \text{(A.2-6)}$$

where

σ_{wd}^2 = variance of the apparent wander distance

Total Measurement Noise The total measurement noise variance is the sum of the variances of the individual uncorrelated noise components,

$$\sigma_\theta^2 = \sigma_r^2 + \sigma^2 + \sigma_s^2 \qquad \text{(A.2-7)}$$

As previously noted, receiver and range independent noise are generally assumed wide-band relative to the guidance system bandwidth. Angular scintillation noise is in general a narrow band source and is often modeled as white noise through a low pass filter with a time constant which depends primarily on the target motion spectrum. On the other hand, if for a radar seeker the radar frequency is changed in a pseudo-random manner from sample-to-sample so as to reduce the ability of the enemy to jam

the missile receiver, then the apparent centroid of target radiation will tend to be independent from sample-to-sample. It will be assumed that all three noise sources are independent and wide-band relative to the guidance system bandwidth.

A.3 AUTOPILOT MODULE

The function of the autopilot subsystem is three-fold; it provides the required missile lateral acceleration response characteristics, it must stabilize or damp the bare airframe, and it reduces the missile performance sensitivity to disturbance inputs over the required flight envelope.

The autopilot configuration illustrated in Fig. A.3-1 uses accelerometer feedback so as to control the lateral acceleration of the missile. Lateral acceleration control is used in accordance with the proportional navigation guidance law which requires a missile lateral acceleration proportional to the measured missile-to-target line-of-sight rotation rate. The body mounted rate gyro senses body attitude rate, $\dot{\theta}_m$, which is used by the autopilot to increase the effective damping ratio of the airframe short period poles.

The aerodynamic characteristics of the missile airframe are an integral part of the autopilot design and operation. Therefore, the design of an autopilot must be tailored to each individual missile airframe configuration and its associated aerodynamic characteristics, which are nonlinear functions of missile velocity, angle-of-attack, control surface deflection and altitude.

It is standard practice in the design of missile autopilots to utilize the linearized second order airframe model given in Chapter 8 of

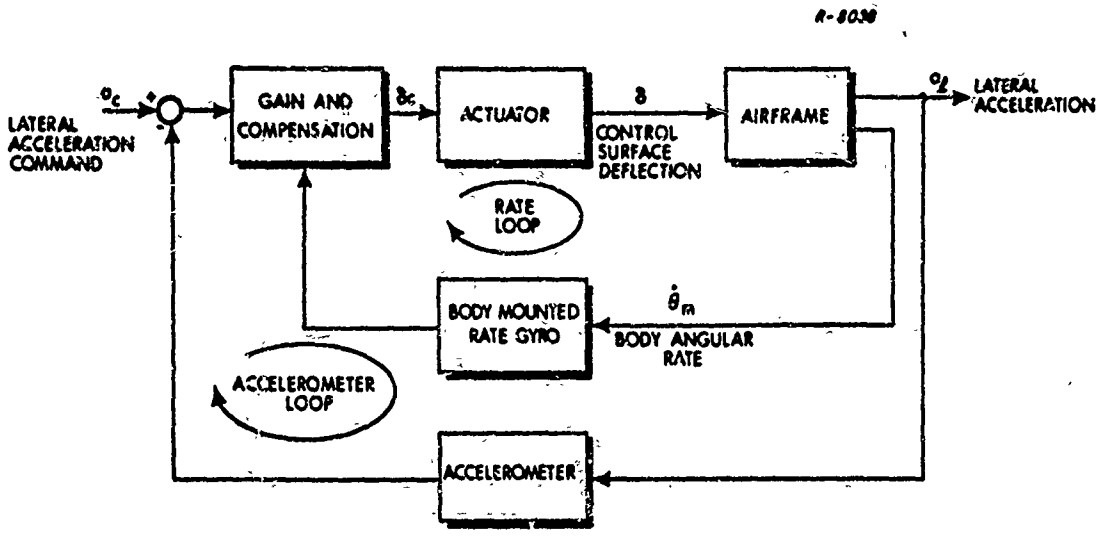

Figure A.3-1 General Missile Autopilot Configuration

Ref. 5. The required stability derivatives are obtained from the non-linear moment and force coefficients by making the following assumptions:

- Constant missile velocity
- Body lift force is a linear function of the change in angle of attack, α, about some trim condition, α_0
- Constant altitude
- Constant center of pressure
- Fixed missile mass and inertia
- Control surface lift force is a linear function of control surface deflection angle, δ, and independent of α

Although the above assumptions appear to be rather restrictive, they simplify the autopilot design task considerably. Practical experience has shown that the resulting autopilot response characteristics with the

nonlinear airframe, are closely approximated by the linearized response characteristics near the given nominal conditions, for a properly designed autopilot. In this report, a realistic autopilot model is developed which requires knowledge of very few specific aerodynamic parameters, yet its response characteristics are easily related to the important missile aerodynamic properties.

Acceleration Command Limiting – The most important nonlinear characteristic associated with the airframe is acceleration saturation, which occurs when the missile attempts to pull a large angle of attack. It is desirable to avoid a large angle of attack since the associated drag results in a rapid loss of missile velocity. There is also the airframe structural limit which must not be exceeded. It is common practice to limit the commanded lateral acceleration so as to prevent both angle-of-attack saturation and structural failure. Therefore, autopilot command limiting is assumed to be the dominant nonlinear effect and all other nonlinear characteristics such as actuator angle and angle rate limiting, aerodynamic nonlinearities, instrumentation nonlinearities, etc., are assumed to be secondary or equivalently represented as acceleration limiting, or as changes in autopilot dynamics. The resulting model is simple and generally applicable to a wide range of missile systems, and captures what is known to be a dominant nonlinear system characteristic and an important factor in miss distance performance--lateral acceleration saturation.

Linear Autopilot Response Characteristics – Using a linearized airframe model (Ref. 5), the closed loop transfer function for the general autopilot configuration of Fig. A.3-1 can be developed for specific gains and compensation, an example of which is given in Fig. A.3-2. The linearized airframe transfer functions, as given by Eq. (8.1-1) of Ref. 5, are:

$$G_1 = \frac{a_\ell}{\delta} = k_1 (1 + a_1 s + a_2 s^2)/\Delta \qquad \text{(A.3-1)}$$

$$G_2 = \frac{a_a}{\delta} \cong G_1 \qquad \text{(A.3-2)}$$

$$G_3 = \frac{\dot{\theta}_m}{\delta} = k_3 (1 + a_3 s)/\Delta \qquad \text{(A.3-3)}$$

$$\Delta = 1 + \frac{2\xi_a}{\omega_a} s + \frac{s^2}{\omega_a^2} \qquad \text{(A.3-4)}$$

R-8043

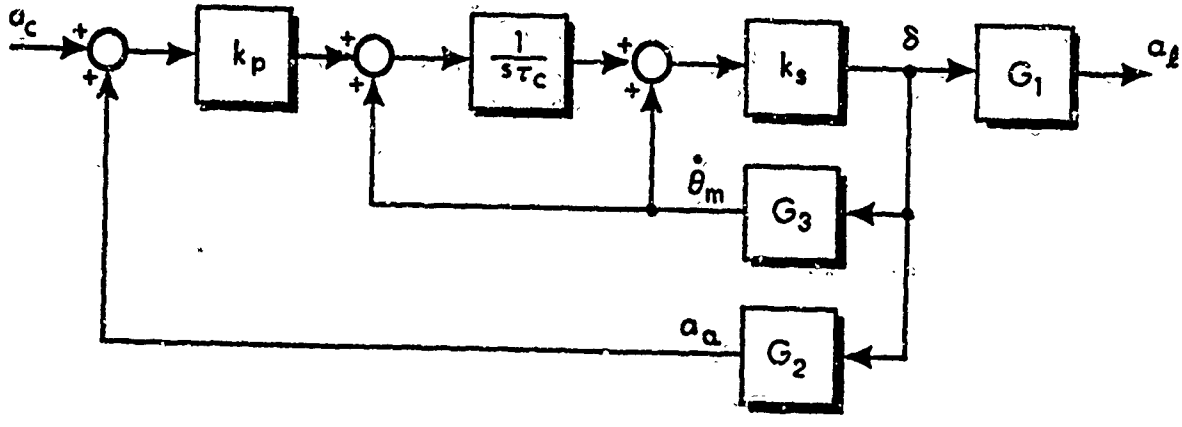

Figure A.3-2 Linear Autopilot Block Diagram

where

ω_a = bare airframe natural frequency

ξ_a = bare airframe damping ratio

a_ℓ = developed lateral acceleration

a_a = measured lateral acceleration

$\dot{\theta}_m$ = body attitude rate

δ = control surface deflection

a_i = transfer function parameters obtained from linearized aero-data and given in Eq. (8.1-8) of Ref. 5.

The G_2 transfer function in Eq. (A.3-2) will be assumed equal to G_1; this is true if the accelerometer is located at the c.g. of the missile and has a wide bandwidth. The actuator dynamics are assumed to be at a frequency which is much higher than the crossover frequency of the rate loop and will therefore be ignored.

Using Eqs. (A.3-2) through (A.3-4) the closed loop transfer function from commanded to developed lateral acceleration Fig. A.3-2 is

$$\frac{a_\ell}{a_c} = k_c \left[\frac{1 + a_1 s + a_2 s^2}{1 + b_1 s + b_2 s^2 + b_3 s^3} \right] \qquad (A.3\text{-}5)$$

$$= k_c \left[\frac{1 + a_1 s + a_2 s^2}{\left(1 + \frac{s}{\omega_1}\right)\left(1 + \frac{2\xi_2 s}{\omega_2} + \frac{s^2}{\omega_2^2}\right)} \right]$$

where

$$b_1 = \frac{1}{\omega_1} + \frac{2\xi_2}{\omega_2} \qquad \text{(A.3-6)}$$

$$b_2 = \frac{2\xi_2}{\omega_2} + \frac{1}{\omega_2^2} \qquad \text{(A.3-7)}$$

$$b_3 = \frac{1}{\omega_1 \omega_2^2} \qquad \text{(A.3-8)}$$

k_c = closed loop d-c gain in Fig. A.3-2.

In the case of a tail-controlled missile, the transfer function in Eq. (A.3-5) is non-minimum phase...i.e., it has a right-half-plane zero; this produces the "wrong-way" or "tail-wags-dog" effect, discussed in Ref. 5. The transfer function from commanded acceleration to developed body attitude rate is:

$$\frac{\dot{\theta}_m}{a_c} = \frac{k_c}{v_m} \frac{(1 + a_3 s)}{1 + b_2 s + b_2 s^2 + b_3 s^3} \qquad \text{(A.3-9)}$$

where v_m is the missile velocity.

Recall from the discussion in Section A.1 that radome errors can couple body angle rate, $\dot{\theta}_m$, into the LOS measurements. This forms a "parasitic attitude loop" since LOS data is used to form the lateral acceleration command which results in a change of body attitude in Eq. (A.3-9). As this coupling becomes large, guidance stability is compromised and miss distance will tend to increase. An important measure of the required missile attitude rate is a_3, which tends to increase with altitude thus intensifying the parasitic attitude loop problem.

There is a wide range of values that can be selected for ω_1, ω_2 and ξ_2 in Eq. (A.3-5). For many systems it is possible, and desirable where attitude loop stability is a consideration, to design the autopilot such that ω_2 is much larger than ω_1 and $\xi_2 \cong 0.5$. The value of ω_2 depends primarily on the rate loop gain for the assumed configuration of Figure A.3-2. If the actuator bandwith is much larger than the open rate loop crossover frequency, ω_r, which is in turn much larger than the airframe natural frequency, ω_a, then ω_r can be approximated as

$$\omega_r \cong |k_s m_\delta|$$

where k_s is defined in Fig. A.3-2 and m_δ is the pitch-moment-effectiveness of the control surface. The magnitude of m_δ tends to increase with Mach number and decrease with altitude. If k_s is adjusted (adaptively) so as to keep ω_r nearly constant, then under the stated condition, ω_2 and ξ_2 will tend to remain nearly constant over a wide range of altitude and velocity conditions. At altitudes less than 10,000 feet, ω_1 tends to be nearly constant over a wide range of missile Mach numbers. At higher altitudes, ω_1 tends to decrease with increasing altitude and increase with increasing Mach number. However for an assumed constant velocity intercept within a narrow altitude band, ω_1 will remain nearly constant. Therefore, the guidance system truth model will use a constant coefficient autopilot having the assumed form of Eqs. (A.3-5) and (A.3-9), as shown in Fig. A.3-3.

A.4 GEOMETRY MODULE

The general form of the intercept geometry is illustrated in Fig. A.4-1. The reference coordinate system is defined with its x-axis along the original missile-to-target line-of-sight (LOS) defined at the initiation of the terminal phase. It is assumed that missile-target motion

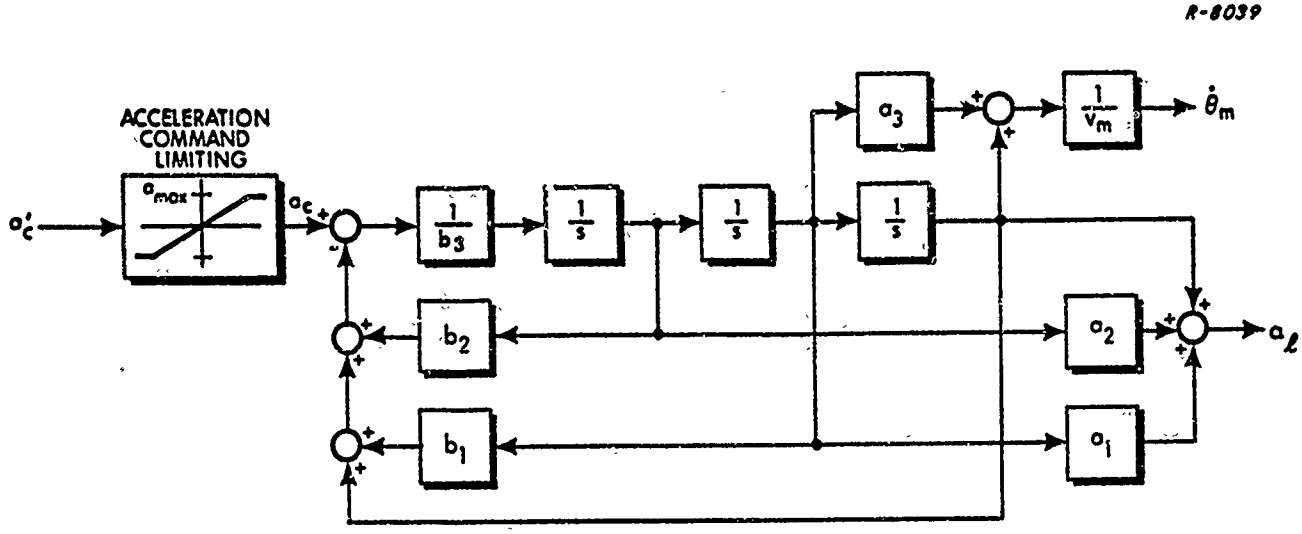

Figure A.3-3 Simulation Autopilot Model

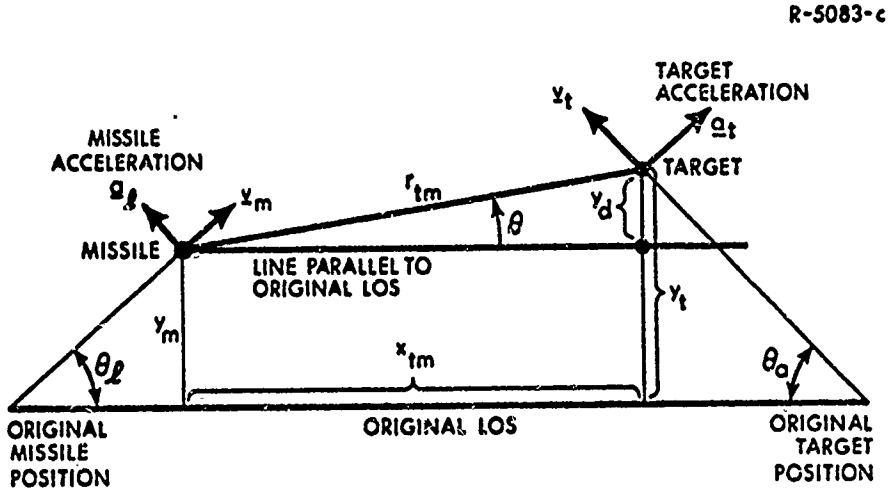

Figure A.4-1 Intercept Geometry

is constrained to the intercept plane, defined by the orthogonal reference x and y axes. The intercept plane can in general assume any orientation with respect to the earth, depending on the initial relative missile and target position and the orientation of their respective velocity vectors. A nominal co-altitude intercept trajectory is assumed herein. This eliminates the specification of an altitude profile and the associated requirement to handle nonstationary altitude dependent aerodynamic characteristics in the autopilot model. It is also assumed that gravity compensation is used in the missile guidance law to negate the effect of gravity on missile performance. Of course, for any orientation of the intercept plane that is not horizontal, there will be an altitude change for motion in the y-direction.

Equations of Motion – As illustrated in Fig. A.4-1, the reference coordinate system is non-rotating but is allowed to translate with the missile. This selection of reference system is dictated primarily by the proportional navigation guidance law which attempts to null the LOS rotation rate, $\dot{\theta}$, by commanding a proportional missile acceleration normal to the LOS. If this guidance scheme works well, θ will remain near its initial zero value and the severity of a number of geometric nonlinearities can be reduced and in many cases linearized.

The missile lead angle, θ_ℓ, and the target aspect angle, θ_a, in Fig. A.4-1 define the orientation of the respective missile and target velocity vectors in the intercept plane relative to the original LOS. Closing velocity, v_c, is defined as the relative velocity measured along the LOS; viz.,

$$v_c = v_m \cos(\theta_\ell + \theta_{he} - \theta) + v_t \cos(\theta_a + \theta) \qquad \text{(A.4-1)}$$

where

v_m = missile velocity
v_t = target velocity
θ_{he} = heading error

Heading error, θ_{he}, is the angular error in the collision-course triangle defined at the initiation of the terminal phase. The sides of the collision-course triangle are established by the closing velocity along the original LOS, the missile velocity vector and the target velocity vector. Given a target aspect angle, θ_a, the collision-course missile lead angle must be

$$\theta_{\ell c} = \sin^{-1}\left[\frac{v_t}{v_m}\sin\theta_a\right] \qquad \text{(A.4-2)}$$

If the orientation and magnitude of the velocity vectors were to remain fixed for the remainder of the terminal phase, the two vehicles would collide. In practice, it is not possible to achieve the collision course lead angle and the difference between $\theta_{\ell c}$ and the actual lead angle θ_ℓ is defined as the heading error. For missile systems having a midcourse phase preceding the terminal phase, heading error tends to be small, having an rms value of a few degrees or less; in a "dog-fight missile" engagement, heading error can be tens of degrees. It is assumed in the following model development that heading error is less than 10 deg.

The missile and target accelerations are assumed to be normal to their respective velocity vectors. In reality, there are also components of acceleration developed along their velocity vectors due to aerodynamic and induced drag which integrate into a net reduction of the velocity vector magnitudes. This is particularly true of the missile after engine burn-out.

However, if it is assumed that drag acceleration is small or a sustainer engine is used to maintain a nearly constant velocity, only the acceleration normal to the velocity vector, a_ℓ, need be considered. Since it will be assumed that the magnitude of the velocity vector is constant, the rate of change of its orientation is proportional to the normal acceleration, resulting in the following expression for lead angle rate:

$$\dot{\theta}_\ell = \frac{a_\ell}{v_m} \qquad \text{(A.4-3)}$$

The analogous expression for target output angle rate due to target acceleration, a_t, normal to its velocity vector is

$$\dot{\theta}_a = \frac{a_t}{v_t} \qquad \text{(A.4-4)}$$

Therefore, the rotation rates of the velocity vectors are proportional to the respective lateral accelerations.

The relative velocity normal to the original LOS, $\dot{y}_d$, is

$$\dot{y}_d = v_t \sin \theta_a - v_m \sin \theta_\ell \qquad \text{(A.4-5)}$$

where

$$\theta_\ell = \frac{1}{v_m} \int_0^t a_\ell \, dt + \theta_{\ell c} + \theta_{he} \qquad \text{(A.4-6)}$$

$$\theta_a = \frac{1}{v_t} \int_0^t a_t \, dt + \theta_{ac} \qquad \text{(A.4-7)}$$

From Fig. A.4-1, θ is given by

$$\theta = \tan^{-1}\left(\frac{y_d}{x_{tm}}\right) \qquad \text{(A.4-8)}$$

where x_{tm} is the missile-to-target range measured along the original LOS. As previously mentioned, θ tends to remain small if the guidance law is operating properly throughout the duration of the terminal phase. However, during the last fraction of a second as intercept is approached, x_{tm} approaches zero and θ will tend to increase for a given value of y_d. With only a fraction of a second left before the end of the flight, there isn't enough time for the missile lateral position to respond to the rapidly increasing LOS angle. In fact, the high LOS rate generally results in saturation of the autopilot acceleration command before θ becomes large. Therefore, for modeling purposes, accurate computation of θ is not required during the period in which it becomes large, thus allowing the small angle approximation of Eq. (A.4-9) to eliminate the $\tan^{-1}$ nonlinear operation.

$$\theta \cong \frac{y_d}{x_{tm}} \text{ (rad)} \qquad \text{(A.4-9)}$$

It is important to note that x_{tm} appears in the denominator of Eq. (A.4-9). Therefore, if x_{tm} is modelled as a system state, it is necessary to handle the associated nonlinear ratio of states. However, if x_{tm} can be modelled as a deterministic quantity which is only a function of time, Eq. (A.4-9) is linear and the computation of θ is considerably simplified. It will be shown in the following paragraph that the difficulties associated with the computation of θ and miss distance are all related to a non-constant closing velocity.

Miss Distance – Miss distance is defined as the point of closest approach between the missile and target, illustrated in Fig. A.4-2, and is given by the relative range when the closing velocity is equal to zero in Eq. (A.4-1). Since closing velocity is defined as the relative velocity between the missile and target projected onto the instantaneous LOS, miss distance is equal to the missile to target range when the inner product of range and range rate is equal to zero, viz.,

$$\text{miss} = |\underline{r}_{tm}| \Big|_{\underline{r}_{tm} \cdot \dot{\underline{r}}_{tm} = 0} \qquad \text{(A.4-10)}$$

where

$\underline{r}_{tm} = x_{tm}\underline{i} + y_d\underline{j}$

$\underline{i}$ = unit vector in the x direction

$\underline{j}$ = unit vector in the y direction

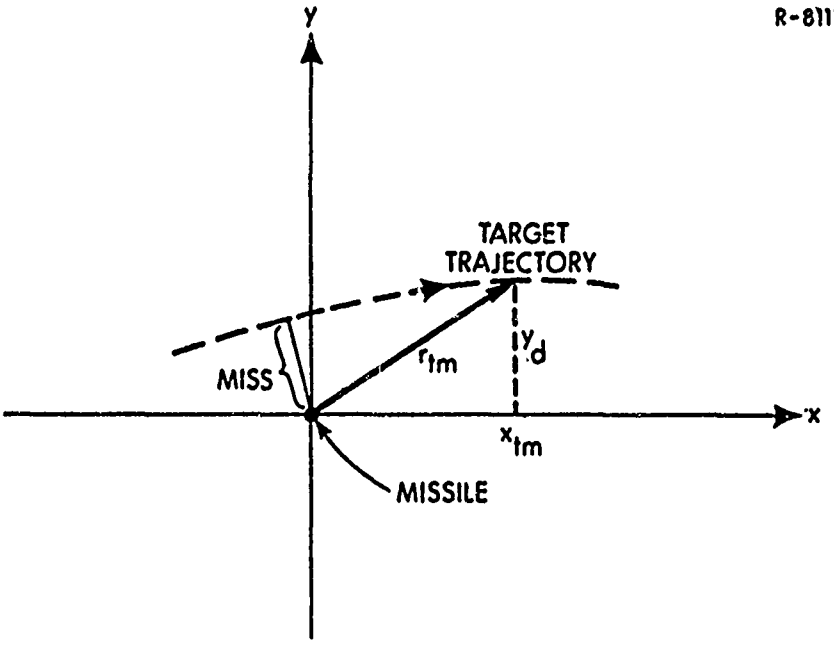

Figure A.4-2 Relative Missile-Target Geometry Near Intercept

At the point in space where the orthogonality of the relative range and velocity vectors required by Eq. (A.4-10) exists, miss distance is given by

$$\text{miss} = y_d \left(- \frac{\dot{y}_d}{\dot{x}_{tm}} \underline{i} + \underline{j} \right) \qquad \text{(A.4-11)}$$

For many intercept situations, $\dot{x}_{tm}$ is much larger than $\dot{y}_d$ in Eq. (A.4-11). Therefore the downrange component of miss distance is neglected in these studies.

Although miss distance is closely approximated by y_d, it (the miss) is defined at only one point during the flight--namely the point of closest approach. Therefore it is conditioned on a spatial rather than a time relationship. In a monte carlo study, the orthogonality condition is tested near the expected end of each flight and y_d is saved when the condition is satisfied. Therefore, if the closing velocity is not constant or there is a significant down range miss component, the time-of-flight at which miss distance is measured will not be constant from one trial to the next. The ensemble miss distance statistics are computed using the "saved" values of miss distance, each of which occurs at a different time of flight. By contrast, the covariance analysis technique provides ensemble performance statistics as a function of time. Therefore, additional computations or approximations are required to obtain miss distance using the covariance analysis approach.

The primary contributor to a nonconstant time-of-flight, for a given initial range, is the fact that the closing velocity in Eq. (A.4-1) is not constant. Since it has already been assumed that the magnitudes of the missile and target velocity vectors ar constant, any change in $\dot{y}_d$ is a result of the change in the orientation of the velocity vectors. However, if the change in these angles is assumed to be small during the flight, the closing velocity will remain nearly constant except as the point of minimum range is approached where it rapidly approaches zero. The projec-

tion of missile and target velocity onto the original LOS, $\dot{x}_{tm}$, will also be nearly constant throughout the flight. Therefore, $\dot{x}_{tm}$ is assumed to be a deterministic quantity which goes to zero at a known fixed time. This assumption eliminates the previously mentioned computational problem associated with θ in Eq. (A.4-9).

From Eq. (A.4-10) it follows that miss is defined when

$$x_{tm} = - \frac{y_d \dot{y}_d}{\dot{x}_{tm}} \qquad \text{(A.4-12)}$$

The incremental time, Δ_t, between when Eq. (A.4-12) is satisfied and x_{tm} is equal to zero is approximated by simply dividing Eq. (A.4-12) by $\dot{x}_{tm}$.

$$\Delta_t = - \frac{y_d \dot{y}_d}{\dot{x}_{tm}^2} \qquad \text{(A.4-13)}$$

For most intercepts, Δ_t is on the order of milliseconds. The change in y_d over such a small interval is negligible and miss distance can be approximated as y_d measured when x_{tm} equals zero.

A.5 TARGET MODULE

The target velocity vector is assumed to have a constant magnitude, and a direction described by θ_a in Fig. (A.4-1). It is further assumed that the target may have random changes in its acceleration normal to its velocity vector. The assumed acceleration time history model is a randomly reversing poisson square wave as illustrated in Fig. A.5-1. This square wave switches between $\pm\beta$ ft/sec^2 with random

poisson distributed switching times having an average of ν zero-crossings per second. The autocorrelation function (Ref. 9) for observation times t_a and t_b is

$$\varphi(t_a - t_b) = \beta^2 e^{-2\nu|t_a - t_b|} \qquad \text{(A.5-1)}$$

Equation (A.5-1) indicates that the mean-squared value of a_t is β^2 and, as ν approaches zero, a_t approaches a constant. The power spectral density associated with a_t is

$$\Phi(\omega) = 2\lambda_t \beta^2 \left[\frac{1}{\lambda_t^2 + \omega^2} \right] \qquad \text{(A.5-2)}$$

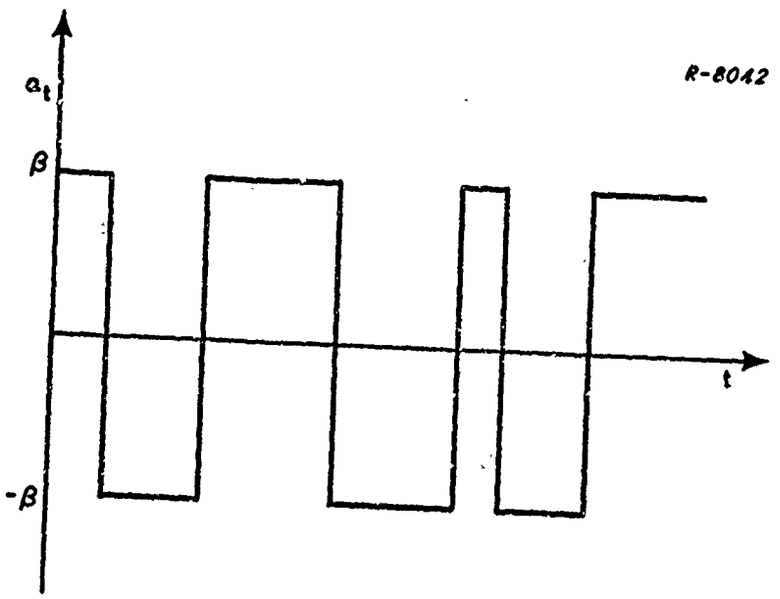

Figure A.5-1 Poisson Square Wave for Target Acceleration

where λ_t is defined as the maneuver bandwidth and is equal to 2ν. The resulting maneuver model has the same mean and autocorrelation function as a first-order markov process. Therefore, the target lateral maneuver acceleration will be modelled as the output of a low pass filter with bandwidth λ_t driven by white noise with a power spectral density of $2\lambda\beta^2$, resulting in a rms acceleration level of β.

It is interesting to note that although the autocorrelation function and the corresponding power spectral density for the poisson square wave are identical to that of a markov process, the associated probability density functions can be quite different. It is obvious from Fig. A.5-1 that the poisson square wave can only take on values of $\pm\beta$. The resulting bi-polar amplitude probability density function consists of impulses with a weighting of 0.5 at plus and minus β whereas the markov process is generally assumed to have a gaussian amplitude distribution. Therefore, the response of an amplitude dependent nonlinear operator could be quite different when driven by each of these two signal forms. However, if the random square wave is passed through a narrow band filter or integrator, it would experience rounding due to the finite bandwidth. In the case of an integrator, the resulting wave shape would be a series of constant slope segments. By application of the central limit theorm, as illustrated in Ref. 8*, the resulting output distribution approaches the gaussian density function.

*page 179

A.6 GUIDANCE MODULE

The operation of the guidance module may be separated into two cascaded functions: 1) filtering of the noisy measurements obtained from the seeker and 2) utilization of the filtered measurements to control the missile lateral acceleration. There are a number of filtering and control schemes that can be used by tactical missiles, as reported in Refs. 5 and 7. However, the current study will be limited to the configurations listed in Table 2.2-1; each of these is discussed below.

Configuration A – This configuration can be considered as the classical approach to missile guidance. The boresight error signal from the seeker module is processed through a constant bandwidth low-pass noise filter. For modelling purposes, it is assumed that the measurement rate is much faster than the noise filter bandwidth. The resulting system can therefore be characterized by a continuous model which is representative of a missile with either an analog on-board signal processor or a digital unit with a high cycle rate. This system can also be considered as one of minimum complexity.

The boresight error signal obtained from the seeker module is a noisy measurement of LOS rate at frequencies below that of the seeker track-loop bandwidth. Therefore, the output of the guidance noise filter is also a band-limited indication of LOS rate. Classical proportional guidance requires the development of a lateral acceleration of the missile normal to the LOS, which is proportional to the LOS rate as given by

$$a_\ell = \frac{n' v_c}{\cos(\theta_\ell - \theta)} \dot{\theta} \qquad \text{(A.6-1)}$$

where

v_c = closing velocity (ft/sec)

$\dot{\theta}$ = LOS rate (rad/sec)

θ = LOS angle (rad)

n' = navigation ratio

θ_ℓ = lead angle (rad)

The proportionality factor is comprised of the navigation ratio, closing velocity multiplier and a geometric gain factor which accounts for the fact that the orientation of the missile velocity vector is not necessarily along the instantaneous LOS. Since missile lateral acceleration is developed normal to its velocity vector, it must be increased by the indicated factor so the projection normal to the LOS will be proportional to $\dot{\theta}$.

In practice, neither θ or θ_ℓ are directly available for use by the guidance module. If the guidance law is operating properly, θ will be small for all but the last fraction of a second before intercept. If the variation of the lead angle is small, then the factor of proportionality can be considered constant for all practical purposes. (This is also consistent with the assumption of a constant closing velocity in the geometry module). Some missile systems use the gimbal angle, θ_h, to approximate $(\theta_\ell - \theta)$ or simply enter a constant which is representative of the average value. In this study, a constant value will be used in the truth model; any error in this value can be accounted for as an effective change in the navigation ratio. The resulting block diagram for Guidance Law A is given in Fig. A.6-1.

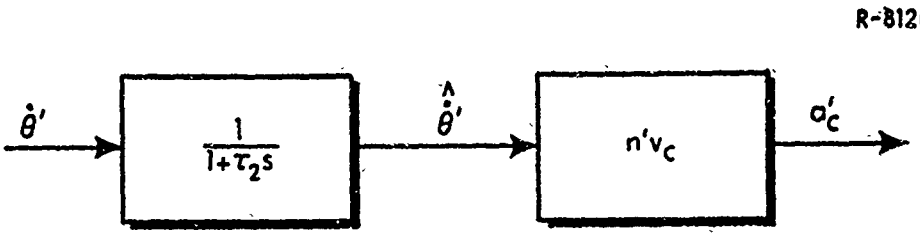

Figure A.6-1 Guidance Law A

Kalman Filter for Configurations B, C, D and E – The Kalman filter is implemented in the non-rotating, initial LOS coordinate system. For the purpose of designating the filter, it is assumed that both the target and missile maneuver with their accelerations normal to the initial LOS; the resulting plant model for the Kalman filter is given in Fig. A.6-2.

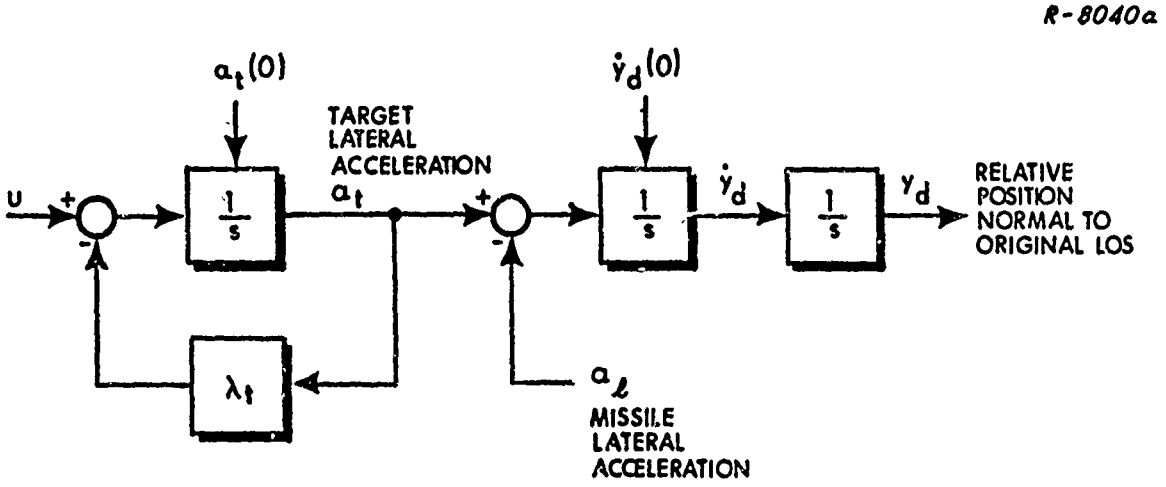

Figure A.6-2 Kalman Filter Plant Model

In state-space notation, the filter model equations of motion are given by the vector differential equation

$$\dot{\underline{x}}(t) = F\underline{x}(t) + \underline{u}(t) + \underline{b}(t) \qquad \text{(A.6-2)}$$

where

$$\underline{x} = \begin{bmatrix} y_d \\ \dot{y}_d \\ a_t \end{bmatrix} \qquad F = \begin{bmatrix} 0 & 1 & 0 \\ 0 & 0 & 1 \\ 0 & 0 & -\lambda_t \end{bmatrix}$$

$$\underline{b} \quad \begin{bmatrix} 0 \\ -a_\ell \\ 0 \end{bmatrix} \qquad Q = \begin{bmatrix} 0 & 0 & 0 \\ 0 & 0 & 0 \\ 0 & 0 & 2\lambda_t \beta^2 \end{bmatrix}$$

$$E\left\{u(t)\, u^T(\tau)\right\} = Q\,\delta(t-\tau)$$

$$E\left\{\underline{x}(0)\, \underline{x}^T(0)\right\} = P(0) = \begin{bmatrix} 0 & 0 & 0 \\ 0 & \overline{\dot{y}_d^2(0)} & 0 \\ 0 & 0 & \overline{a_t^2(0)} \end{bmatrix}$$

Note that this model is identical to the system truth model used in the target and geometry modules with the exception that target and missile acceleration are assumed normal to the orginal LOS. The system truth model is more exact in that the missile and target lateral accelerations are assumed to be normal to their respective velocity vectors, which in

general do not lie along the original LOS. Furthermore, for the purpose of mechanizing the filter, it is assumed that the autopilot output a_ℓ can be measured without error.

The measurement to be processed by the Kalman filter is the sampled LOS angle θ', having additive independent samples of noise v_k. The latter have zero mean and variance given by

$$E\left\{v_k^2\right\} = \sigma_r^2(t_k) + \sigma^2 + \sigma_s^2(t_k) \triangleq R_k$$

where σ_r, σ, and σ_s represent the noise components defined in Section A.2. In terms of the state vector $\underline{x}$ in Eq. (A.6-2), the LOS angle measurement is expressed as

$$z_k = \underline{h}^T(t_k)\,\underline{x}_k + v_k$$

$$\underline{h}^T(t) = \left[\frac{1}{r_{tm}(t)} \quad 0 \quad 0\right] \qquad \text{(A.6-3)}$$

The discrete Kalman filter mechanization equations have the form

$$\dot{\underline{\hat{x}}}(t) = F\underline{\hat{x}}(t) + \underline{b}(t); \text{ between measurements} \qquad \text{(A.6-4)}$$

$$\underline{\hat{x}}_k = \underline{\hat{x}}_k^- + \underline{k}_k\left(z_k - \underline{h}^T(t_k)\,\underline{\hat{x}}_k^-\right); \text{ at a measurement} \qquad \text{(A.6-5)}$$

where $\underline{\hat{x}}_k^-$ denotes the solution to Eq. (A.6-4) just before a measurement is processed. The gain vector $\underline{k}_k$ is obtained recursively from the matrix covariance equation associated with the Kalman filter;

$$\underline{k}_k = M_k \underline{h}_k \left(\underline{h}_k^T M_k \underline{h}_k + R_k \right)^{-1}$$

$$M_k = \Phi P_{k-1} \Phi^T + Q_s$$

$$P_k = M_k - \underline{k}_k \left(\underline{h}_k^T M_k \underline{h}_k + R_k \right) \underline{k}_k^T$$

$$Q_s = \int_0^{\Delta t} e^{F(\Delta t - \tau)} Q \left[e^{F(\Delta t - \tau)} \right]^T d\tau$$

$$P_0 = E \left\{ \underline{x}(0) \underline{x}(0)^T \right\} \Phi = e^{F \Delta t} \qquad \text{(A.6-6)}$$

The gains cannot be precomputed and stored because $\underline{h}$ and R in Eqs. (A.6-6) are range dependent; this requirement is responsible for most of the digital computational capability required by the guidance system.

The mechanization of the Kalman filter is illustrated in Fig. A.6-3 where $\hat{y}_d$, $\hat{\dot{y}}_d$ and a_t are the respective estimates of y_d, $\dot{y}_d$ and a_t. Discrete updates of the estimates occur when the sampler closes. Between updates, the estimates simply propagate according to the modelled dynamics. The gains k_{1k}, k_{2k} and k_{3k} are the elements of $\underline{k}_k$ in Eqs. (A.6-6).

The initial covariance matrix P (0) used in the computation of the Kalman gains contains two non-zero elements. The initial value of its third diagonal element, p_{33}, is the variance of the target acceleration at the initiation of the terminal phase. It will be assumed that the target has been maneuvering prior to the start of terminal phase and

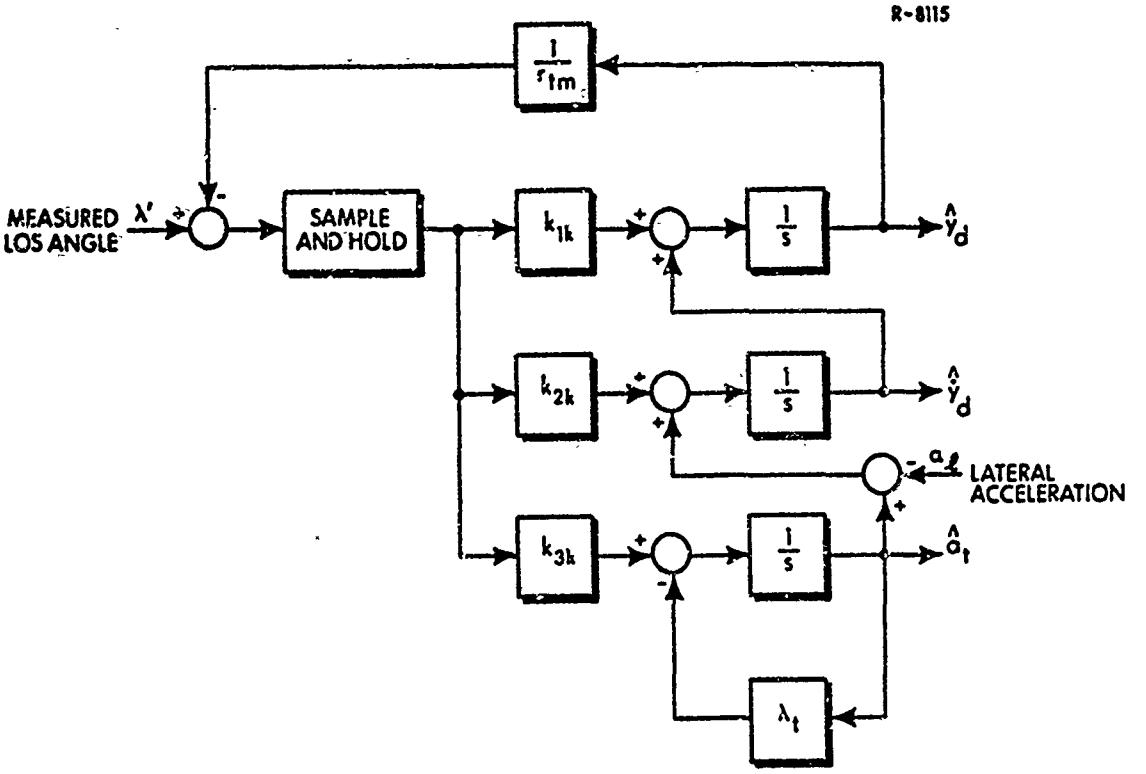

Figure A.6-3 Kalman Filter Mechanization Diagram

the initial variance is equal to the steady-state maneuver level, β^2 (Eq. A.5-1). The initial value of the second diagonal element of P, p_{22}, is equal to the variance of the relative velocity normal to the initial LOS at the initiation of the terminal phase. From Eq. (A.4-5) of Section A.4, it can be shown that the initial value of $\dot{y}_d$ is approximated by

$$\dot{y}_d(0) \cong - \theta_{he} v_m \qquad \text{(A.6-7)}$$

for small values of initial heading error, θ_h. Therefore, since v_m is assumed to be a true constant,

$$p_{22}(0) = \sigma_{he}^2 v_m^2 \qquad \text{(A.6-8)}$$

where σ_{he} is the standard deviation of initial heading error.

Controller for Guidance Laws B, C, and D– The control input to be determined is the commanded missile lateral acceleration in Fig. A.3-3 . Continuous control will be assumed in deriving the guidance laws and it is desired to minimize the expected square of the miss distance subject to a penalty function on the total control energy. Therefore, the performance index to be minimized is given by

$$J = y_d^2(t_f) + \gamma \int_0^{t_f} a_c'(t)^2 \, dt \qquad \text{(A.6-9)}$$

subject to the equations of motion in Eq. (A.6-2) and the autopilot dynamics modeled by the first order transfer function

$$\frac{a_\ell}{a_c'} = \frac{a_\ell}{a_c} = \frac{\lambda_m}{s + \lambda_m} \qquad \text{(A.6-10)}$$

Note that the saturation in Fig. A.3-3 is neglected in Eq. (A.6-10), as well as the higher-order autopilot dynamics. The quantities $y_d(t_f)$ and γ are respectively the terminal miss distance at intercept time t_f and the weighting on control effort. The solution to this problem is called an optimal guidance law. By invoking the separation principle (Ref. 10) it is known that the control will be of the form

$$a_c' = c_1 \hat{y}_d + c_2 \hat{\dot{y}}_d + c_3 \hat{a}_t + c_4 a_\ell \qquad \text{(A.6.11)}$$

The indicated control gains, which minimize the performance index in Eq. (A.6-9), have been determined by Willems in Ref. 2 and are repeated below for convenience (t_{go} is the time until intercept):

$$c_1 = \frac{n'}{t_{go}^2} \qquad \text{(A.6-12)}$$

$$c_2 = \frac{n'}{t_{go}} \qquad \text{(A.6-13)}$$

$$c_3 = n'\left[\frac{e^{-\lambda_t t_{go}} + \lambda_t t_{go} - 1}{\lambda_t^2 t_{go}^2}\right] \qquad \text{(A.6-14)}$$

$$c_4 = -n'\left[\frac{e^{-\lambda_m t_{go}} + \lambda_m t_{go} - 1}{\lambda_m^2 t_{go}^2}\right] \qquad \text{(A.6-15)}$$

The optimal navigation ratio, n', is given by

$$n' = \frac{3t_{go}^2\left[t_{go} - \left(1 - e^{-\lambda_m t_{go}}\right)/\lambda_m\right]}{3\gamma + \frac{3}{2\lambda_m^3}\left(1 - e^{-2\lambda_m t_{go}}\right) + \frac{3t_{go}}{\lambda_m^2}\left(1 - 2e^{-\lambda_m t_{go}}\right) + t_{go}^2\left(t_{go} - \frac{3}{\lambda_m}\right)} \qquad \text{(A.6-16)}$$

The expression for n' is considerably simplified as λ_m approaches infinity; i.e.,

$$n'\Big|_{\lambda_m = \infty} = \frac{3t_{go}^3}{3\gamma + t_{go}^3} \qquad \text{(A.6-17)}$$

If there is no constraint on acceleration, γ is equal to zero and the resulting navigation ratio from Eq. (A.6-17) is constant with a value of 3. The optimal navigation ratio from Eq. (A.6-16) tends to increase as t_{go} approaches zero. If γ is equal to zero, n' will approach extremely large values as t_{go} approaches zero. However, for a non-zero value of γ, n' will first increase as t_{go} becomes small; after a point it will begin

to decrease with t_{go}, and finally approach zero as t_{go} goes to zero. This nonstationary behavior of the navigation ratio becomes more pronounced as λ_m becomes small. Increasing n' results in a direct scaling of all four control gains, which in turn increases the autopilot command, a_c, to compensate for the dynamic lag represented by Eq. (A.6-10).

Given this set of optimal linear control gains, various suboptimal approximations can be made to simplify the computational requirements. If γ, $1/\lambda_m$, c_3 and c_4 are arbitrarily set to zero, classical proportional navigation with $n' = 3$ (Guidance Law B) is the resulting control policy. This is shown by differentiating the expression for LOS angle,

$$\theta \cong \frac{y_d}{x_{mt}} \tag{A.6-18}$$

to obtain

$$\dot{\theta} = \frac{\dot{y}_d x_{mt} - y_d \dot{x}_{mt}}{x_{mt}^2} \tag{A.6-19}$$

For the assumed constant closing velocity intercept,

$$\dot{x}_{mt} = v_c t_{go} \tag{A.6-20}$$

and Eq. (A.6-19) becomes

$$\dot{\theta} = \frac{1}{v_c}\left[\frac{\dot{y}_d}{t_{go}} + \frac{y_d}{t_{go}^2}\right] \tag{A.6-21}$$

Classical proportional navigation is defined as

$$a_c' = n' v_c \dot{\theta} \qquad \text{(A.6-22)}$$

Substituting Eq. (A.6-21) for $\dot{\theta}$ in Eq. (A.6-22) and replacing $\dot{y}_d$ and y_d by their best estimates, obtained from the Kalman filter, yields

$$a' = n' \left[\frac{\hat{\dot{y}}_d}{t_{go}} + \frac{\hat{y}_d}{t_{go}} \right] \qquad \text{(A.6-23)}$$

Comparing Eq. (A.6-23) with Eqs. (A.6-11), (A.6-12), (A.6-13), and (A.6-17) proves the equivalence between proportional navigation and the optimal guidance law under the conditions $1/\lambda_m = \gamma = c_3 = c_4 = 0$. The navigation ratio is held constant in Eq. (A.6-23). Guidance Law C is obtained by including a component of target acceleration in the formulation of the autopilot command via c_3. Finally, Guidance Law D is realized by including $1/\lambda_m \neq 0$ in the computation of n', as well as the term involving c_4 in Eq. (A.6-11). In all cases investigated here the weighting, γ, on the control penalty in Eq. (A.6-9) is set equal to zero.

Optimal Nonlinear Controller – The optimal nonlinear guidance law is based upon the same system model used for the optimal linear laws described above; however its performance objective is different. Namely, an acceleration command is sought such that

$$J = E\left\{ |\text{miss distance}| \right\} \qquad \text{(A.6-24)}$$

is minimized, subject to the constraint

$$|a_c| \leq a_{max} \qquad \text{(A.6-25)}$$

where a_{max} is the maximum airframe acceleration. Thus the limit on missile acceleration capability is incorporated explicitly into the problem formulation; this is contrasted with the quadratic integral penalty term on a'_c (t) in Eq. (A.6-9).

The solution to the above problem is derived in Refs. 7 and 11. The resulting optimal nonlinear guidance law has the same structure as the linear laws discussed previously; however, the control gains c_1, c_2, c_3 and c_4 are computed differently. The latter are obtained at each control computation stage as a result of the following steps:

- Determine the predicted terminal miss distance based on the Kalman filter estimate of the state vector at the current control computation stage, and the dynamic model defined in Eqs. (A.6-2) and (A.6-10).
- Determine the value of commanded acceleration, a'_c, required over a single control interval to null the predicted terminal miss distance, neglecting the constraint in Eq. (A.6-25).
- Determine the actual acceleration command, a_c, by passing a'_c through a saturation function that satisfies Eq. (A.6-25).

To carry out the above calculations, we first combine Eqs. (A.6-2) and (A.6-10) into the form

$$\dot{\underline{x}}(t) = \tilde{F}\underline{x}(t) + \tilde{\underline{b}}\, a_c(t) \qquad \text{(A.6-26)}$$

where

$$\tilde{F} = \begin{bmatrix} 0 & 1 & 0 & 0 \\ 0 & 0 & 1 & -1 \\ 0 & 0 & -\lambda_t & 0 \\ 0 & 0 & 0 & -\lambda_m \end{bmatrix}; \quad \tilde{\underline{b}} = \begin{bmatrix} 0 \\ 0 \\ 0 \\ \lambda_m \end{bmatrix} \qquad \text{(A.6-27)}$$

*The law is called an optimal nonlinear law because the nonlinear constraint on a_c is incorporated in the problem formulation.

The predicted terminal miss based on a state estimate at time t is given by

$$\hat{y}_d(t_f) = \underline{\tilde{\varphi}}^T(t_f, t)\,\underline{\hat{x}}(t) \qquad \text{(A.6-28)}$$

where $\underline{\tilde{\varphi}}^T(t_f,t)$ is the first row of the state transition matrix corresponding to F in Eq. (A.6-27). The effect of a constant command a_c', applied over an interval Δt, on the terminal miss distance is given by

$$\Delta\hat{y}_d(t_f) = \underline{\tilde{\varphi}}^T(t_f,\ t+\Delta t)\int_t^{t+\Delta t}\tilde{\Phi}(t+\Delta t,\ \tau)\underline{b}\ a_c'\,d\tau$$

$$\triangleq \delta_c(t)\,a_c' \qquad \text{(A.6-29)}$$

The objective is to select a_c' such that

$$\Delta\,\hat{y}_d(t_f) \stackrel{*}{=} -\hat{y}_d(t_f) \qquad \text{(A.6-30)}$$

in order to null the predicted miss distance. Substituting from Eqs. (A.6-28) and (A.6-29) leads to the result

$$a_c' = -\frac{1}{\delta_c(t)}\cdot\underline{\tilde{\varphi}}^T(t_f, t)\,\underline{\hat{x}}(t)$$

$$\triangleq -\left[c_2\hat{y}_d + c_2\dot{\hat{y}}_d + c_3\hat{a}_t + c_4 a_\ell\right] \qquad \text{(A.6-31)}$$

Carrying out the computation for c_1 through c_4 we find that they are the same as in Eqs. (A.6-12) through (A.6-15) except that the navigation ratio n' is given by

$$n' = \frac{-t_{go}^2}{\Delta t\left(\frac{1}{\lambda_m} - t_{go} + \frac{\Delta t}{2}\right) - \frac{1}{\lambda_m^2} e^{-\lambda_m(t_{go}-\Delta t)}\left(1 - e^{-\lambda_m \Delta t}\right)} \quad \text{(A.6-32)}$$

The values of n'given by Eqs. (A.6-16) and (A.6-32) behave quite differently as functions of t_{go}, as demonstrated in Fig. A.6-4. The explanation for this is that the nonlinear law attempts to completely null the predicted miss at each control stage; this requires much larger missile acceleration early in the trajectory than the linear laws, which tend to reduce the predicted miss distance more gradually. The nonlinear law has a smaller gain near intercept because it reduces the miss distance faster than the linear law.

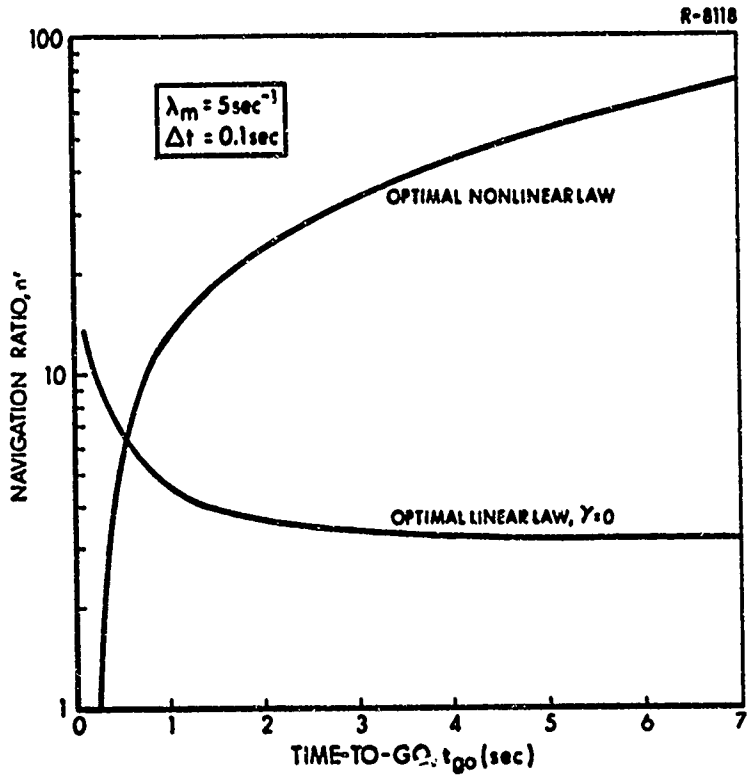

Figure A.6-4 Comparison of Navigation Ratios for Optimal Linear and Nonlinear Laws

Autopilot Command – The autopilot acceleration command given by Eq. (A.6-11) will in practice be contained in the output register of a digital computer. The value of this command will change at discrete intervals which are nearly coincident with the LOS measurements processed by the Kalman filter. In practice there will be a transport lag between the LOS measurement and the update of the control signal due to the computer processing time requirements. It will be assumed that the time delay is small compared to the sampling period and will be neglected. Since the control signal changes at the sample instant and is constant between samples, this operation is equivalent to that of a zero-order hold. Therefore, the autopilot and autopilot model are driven by a stair-case signal which is the sampled and held acceleration command given by Eq. (A.6-11).

A.7 COMPUTATIONAL REQUIREMENTS

The computational requirements for the guidance laws discussed in Section A.6 are primarily dictated by the mechanization equations for the Kalman filter in Eq. (A.6-6). Reference 15 provides a guide for estimating the Kalman filter computational requirements, in terms of numbers of additions, multiplications, and logical operations required to complete the processing of each measurement, and the associated memory capacity needed. Logical operations constitute those involved with retrieving variables from memory, storing in memory, reading instructions, etc.; these frequently contribute as much to the total computation time as do the arithmetical (add, multiply, etc.) calculations.

Using the expressions derived in Ref. 15, the following results are obtained:

3-State Kalman Filter Computational Requirements

No. of Multiplications	≅	125
No. of Additions	≅	90
No. of Logical Operation Units	≅	2950
No. of Storage Locations	≅	Programming - 490 Arrays - 60

Representative execution times for a modern minicomputer are: multiplication = 8 μsec; addition = 2 μsec, logical operation unit = 1 μsec. Applying these multiplication factors to the numbers of operations itemized above, and allowing for the use of two 3-state Kalman filters in the 3-dimensional engagement situation, the total execution time per measurement cycle and storage requirements given in Table A.7-1 are obtained. These estimates are conservative in that they do not allow for programming efficiencies that can be gained by accounting for sparse matrices (lots of zero elements) in the Kalman filter equations (Eq. (A.6-6)).

TABLE A.7-1

APPROXIMATE KALMAN FILTER COMPUTER REQUIREMENTS: TWO THREE-STATE FILTERS

Operation	Number Required	Computation Time (μsec)
Addition	180	360
Multiplication	250	2000
Logical (Load, Store, etc.)	5900	5900
TOTAL		8260
Storage Requirement		610 words

APPENDIX B

THE COVARIANCE ANALYSIS DESCRIBING FUNCTION TECHNIQUE (CADET)

The Covariance Analysis Describing Function Technique (CADET) is a method for analytically determining the statistical properties of a nonlinear system, recently developed at The Analytic Sciences Corporation (Ref. 6). The principal advantage of this technique is that it circumvents monte carlo simulations, thereby achieving substantial savings in computer running time. We first motivate the discussion by reviewing covariance analysis methods for linear systems; then we develop an analogous procedure (CADET) for the nonlinear case.

B.1 COVARIANCE ANALYSIS FOR LINEAR SYSTEMS

The dynamics of a linear continuous stochastic system can be represented by a first-order vector-matrix differential equation in which $\underline{x}(t)$ is the system state vector and $\underline{w}(t)$ is a random forcing function,

$$\dot{\underline{x}}(t) = F(t)\,\underline{x}(t) + \underline{w}(t) \qquad \text{(B.1-1)}$$

Figure B.1-1 illustrates the equation. The state vector is composed of any set of quantities sufficient to completely describe the behavior of the system. The forcing function $\underline{w}(t)$ represents disturbances as well as control inputs, that may act upon the system. It can be assumed without

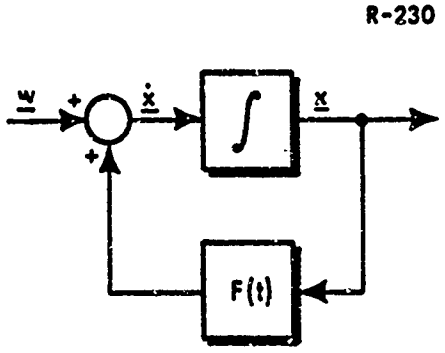

Figure B.1-1 Illustration of Continuous Representation of Linear Dynamic System Equations

loss of generality that the system states and the forcing function are random processes, each having an ensemble average value of zero; i.e., they have zero mean. In what follows the forcing function $\underline{w}(t)$ is assumed to be composed of elements which are uncorrelated in time; that is, $\underline{w}(t)$ is "white" noise having the spectral density matrix $Q(t)$ defined by*

$$E\left[\underline{w}(t)\,\underline{w}(\tau)^T\right] = Q(t)\,\delta(t-\tau)$$

Under the above conditions, the random state can be described in terms of its covariance matrix $P(t)$,

$$P(t) \triangleq E\left[\underline{x}(t)\,\underline{x}(t)^T\right] \qquad \text{(B.1-2)}$$

The equation for the propagation of the covariance matrix for the system described by Eq. (B.1-1) can be written as (Ref. 10).

$$\dot{P}(t) = F(t)\,P(t) + P(t)\,F(t)^T + Q(t) \qquad \text{(B.1-3)}$$

*E denotes ensemble expectation, or average value; T denotes matrix transpose.

The diagonal elements of $P(t)$ are the mean square values of the state variables; the off-diagonal elements represent the amount of correlation between different state variables.

Equation (B.1-3) provides a direct method for analyzing the statistical properties of $x(t)$. This is to be contrasted with the monte carlo method where many sample trajectories of $\underline{x}(t)$ are calculated from computer-generated random noise, or random numbers in the case of a digital computer. If, using the latter technique, m such trajectories are generated using Eq. (B.1-1)--each denoted by $\underline{x}_k(t), k = 1, \ldots, m$--then $P(t)$ is given approximately by

$$P(t) \cong \hat{P}(t) \triangleq \frac{1}{m} \sum_{k=1}^{m} \underline{x}_k(t) \underline{x}_k(t)^T \qquad \text{(B.1-4)}$$

In the limit as m approaches infinity we have

$$\lim_{m \to \infty} \hat{P}(t) = P(t) \qquad \text{(B.1-5)}$$

Note that Eq. (B.1-3) provides an exact solution for $P(t)$, to within computer integration accuracy, whereas the monte carlo method yields an approximate solution for a finite value of m. Furthermore, Eq. (B.1-3) need be solved only once over the trajectory, whereas Eq. (B.1-1) must be solved many times using the monte carlo technique; consequently the direct analytical method is generally the most efficient technique for analyzing linear systems. Our purpose here is to describe a procedure whereby the statistics of a nonlinear system can be computed approximately using a recursion relationship similar in form to Eq. (B.1-3).

B.2 COVARIANCE ANALYSIS FOR NONLINEAR SYSTEMS

The nonlinear counterpart of Eq. (B.1-1) has the form

$$\dot{\underline{x}}(t) = \underline{f}(\underline{x}(t)) + \underline{w}(t) \qquad \text{B.2-1)}$$

In order to develop a covariance analysis method similar to that used for liniar systems it is desirable to approximate $\underline{f}(\underline{x})$ in Eq. (B.2-1) as a linear operation on $\underline{x}(t)$. In particular, we assume that $\underline{x}(t)$ is composed of a known mean $\hat{\underline{x}}(t)$ and an unbiased additive random component $\underline{r}(t)$,

$$\underline{x}(t) = \hat{\underline{x}}(t) + \underline{r}(t) \qquad \text{(B.2-2)}$$

and we shall seek an approximation to $\underline{f}(\underline{x})$ of the form

$$\underline{y}(t) \triangleq \underline{f}(\underline{x}(t)) \cong \hat{\underline{y}}(t) + N_f(t)\,\underline{r}(t) \qquad \text{(B.2-3)}$$

where $N_f(t)$ and $\hat{\underline{y}}(t)$ are to be specified. The structure of this approximation is illustrated in Fig. B.2-1. If Eq. (B.2-3) is substituted into Eq. (B.2-1), then the equations of motion for $\underline{x}(t)$ become linear;

$$\dot{\underline{x}}(t) = \hat{\underline{y}}(t) + N_f(t)\,(\underline{x}(t) - \hat{\underline{x}}(t)) + \underline{w}(t) \qquad \text{(B.2-4)}$$

Taking the expected value of both sites of Eq. (B.2-4) yields an equation for the propagation of $\hat{\underline{x}}(t)$--namely,

$$\dot{\hat{\underline{x}}}(t) = \hat{\underline{y}}(t) = \hat{\underline{f}}(\underline{x}(t)) \qquad \text{(B.2-5)}$$

Subtracting Eq. (B.2-5) from Eq. (B.2-4) produces an equation for $\underline{r}(t)$ having the same form as Eq. (B.1-1);

$$\dot{\underline{r}}(t) = N_f(t)\,\underline{r}(t) + \underline{w}(t) \qquad \text{(B.2-6)}$$

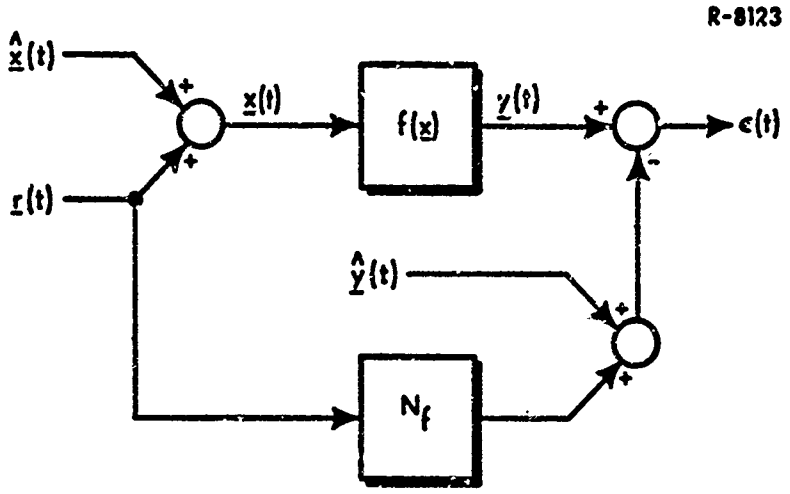

Figure B.2-1 Block Diagram Interpretation of the Linearizing Approximation

Thus by analogy with Eq. (B.1-3), the covariance matrix associated with $\underline{r}(t)$ -- also referred to as the covariance of $\underline{x}$--satisfies the differential equation

$$\dot{P}(t) = N_f(t)\,P(t) + P(t)\,N_f(t)^T + Q(t) \qquad \text{(B.2-7)}$$

Equations (B.2-5) and (B.2-7) together provide the desired analytical description of the statistics of $\underline{x}(t)$--namely its mean value and its covariance matrix--assuming that $\hat{\underline{y}}(t)$ and $N_f(t)$ are known. Subsequent paragraphs discuss the approach taken in CADET for determining these quantities.

Statistical Linearization: The Scalar Case — The method used in CADET for approximating $\underline{f}(\underline{x})$ in Eq. (B.2-1) is based upon statistical

linearization. The basic principle of this technique is conveniently illustrated for a scalar function, f(x), of a random variable x.

Assume that f(x) is to be approximated by the linear expression

$$f(x) \cong n_0 + n_1 x \qquad \text{(B.2-8)}$$

In order to determine appropriate values of the coefficients n_0 and n_1 we define a function representation error, e, of the form

$$e = f(x) - n_0 - n_1 x \qquad \text{(B.2-9)}$$

It is desirable that the coefficients be chosen so that e is small in some "average" sense; the procedure used to accomplish this goal is to minimize the mean square error, $E[e^2]$. Thus, forming

$$E(e^2) = E\left[f^2 + n_0^2 + n_1^2 x^2 - 2n_0 f - 2n_1 fx + 2n_0 n_1 x\right] \qquad \text{(B.2-10)}$$

we require that

$$\frac{\partial E(e^2)}{\partial n_0} = 0$$

$$\frac{\partial E(e^2)}{\partial n_1} = 0 \qquad \text{(B.2-11)}$$

which are necessary conditions for a minimum. Solving Eq. (B.2-11) for n_0 and n_1 produces

$$n_0 = \hat{f} - n_1 \hat{x}$$

$$n_1 = \frac{\widehat{fx} - \hat{f}\hat{x}}{\widehat{x^2} - \hat{x}^2} \qquad \text{(B.2-12)}$$

where the (^) notation denotes expectation. The fact that these values actually minimize the mean square error can be verified by examining the second derivative of $E(e^2)$ with respect to n_0 and n_1. Substituting n_0 from Eq. (B.2-12) into Eq. (B.2-8) produces

$$f(x) \cong \hat{f} + n_1 (x - \hat{x}) \qquad \text{(B.2-13)}$$

Equation (B.2-13) constitutes a statistical linearization of f about the mean value of x because it depends upon the probability density function for x, p(x). That is,

$$\hat{f} = \int_{-\infty}^{\infty} f(x)\, p(x)\, dx$$

$$\widehat{fx} = \int_{-\infty}^{\infty} f(x)\, x\, p(x)\, dx \qquad \text{(B.2-14)}$$

Observe that Eq. (B.2-13) is in the desired form of Eq. (B.2-1) with $\hat{y}$ and N_f identified as the scalar quantities, $\hat{f}$ and n_1 respectively.

The quantity n_1 in Eq. (B.2-12) is usually referred to as the describing function gain. Describing functions are given in Ref. 12 for a wide variety of nonlinear functions with gaussian inputs. From knowledge of n_1 and $\hat{f}$, the statistics of x can be computed using Eqs. (B.2-5) and (B.2-7)--hence the terminology Covariance Analysis Describing Function Technique (CADET).

A more common method of linearizing a nonlinear function is the use of a first-order Taylor series expansion

$$f(x) \cong f(\hat{x}) + \left.\frac{\partial f}{\partial x}\right|_{x=\hat{x}} (x - \hat{x}) \qquad \text{(B.2-15)}$$

In many cases, the CADET procedure tends to be the more accurate approach from a statistical point of view. To demonstrate why this is so consider the example of the saturation nonlinearity in Fig. B.2-2(a) and assume its input has zero mean. If f(x) for this case is expanded in a Taylor series of any order about the origin ($\hat{x} = 0$), we obtain

$$f(x) \cong x \tag{B.2-16}$$

The effect of the saturation is completely lost because of the discontinuity in the first derivative of f. By contrast, if statistical linearization is used, we have

$$f(x) \cong n_1 x \tag{B.7-17}$$

where n_1 is the describing function gain defined by

$$n_1 = \frac{\int_{-\infty}^{\infty} x f(x)\, p(x)\, dx}{\int_{-\infty}^{\infty} x^2\, p(x)\, dx} \tag{B.2-18}$$

and p(x) is the probability density function for x. If we now assume that x is a zero mean gaussian random variable, then

$$p(x) = \frac{1}{\sqrt{2\pi}\sigma}\, e^{-\frac{x^2}{2\sigma^2}} \tag{B.2-19}$$

Substituting Eq. (B.2-19) into Eq. (B.2-18) and evaluating n_1 for the saturation function shown in Fig. B.2-2(a), we obtain (from Ref. 12) the result shown in Fig. B.2-2(b). It can be seen that n_1 is a function

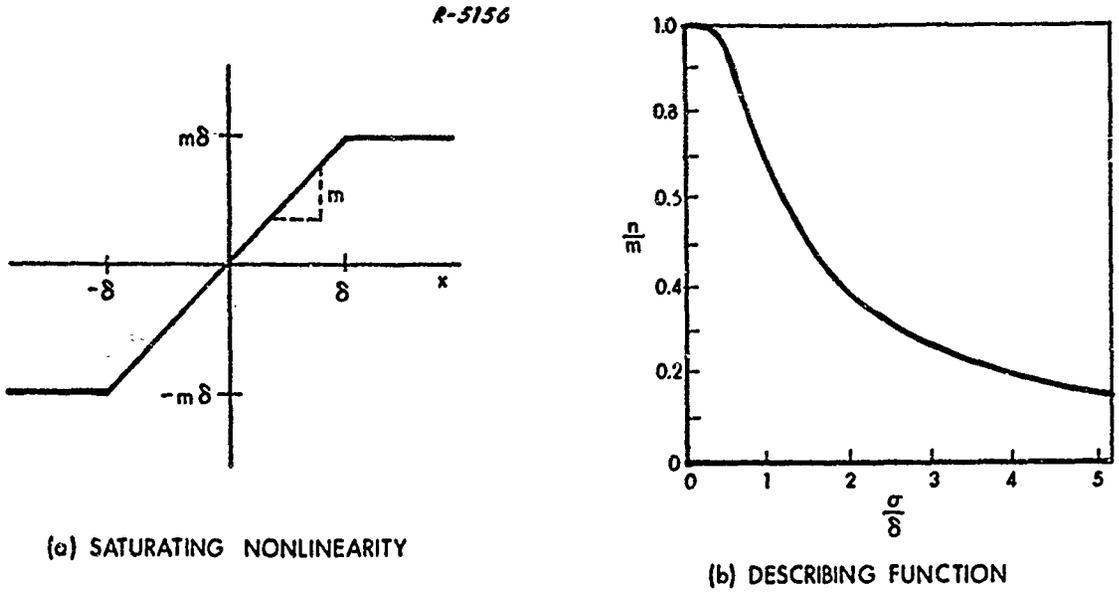

(a) SATURATING NONLINEARITY

(b) DESCRIBING FUNCTION

Figure B.2-2 The Describing Function for a Saturation Nonlinearity (Ref. 12)

of the linear part of f(x), the point δ at which saturation occurs, and the standard deviation of x. The essential feature of the describing function is that it takes into account the probability that x can lie within the saturation region.

For values of σ which are small relative to δ, the probability of saturation is low and n_1 is approximately equal to 1; i.e., f_1 is approximately equal to the Taylor series given in Eq. (B.2-16). For larger values of σ, n_1 is significantly smaller than 1 because there is a higher probability of saturation.

As a result of the above discussion, we can see one distinct advantage that statistical linearization has over the Taylor series expansion; it does not require the existence of derivatives of f(x). Thus, a large number of nonlinearities--relays, saturation, threshold, etc.--

can be treated by this method without having to approximate discontinuities at corners in f(x) by smooth functions. On the other hand, an apparent disadvantage of the method is that the probability density function for x must be known in order to compute $\hat{f}$ and n_1, a requirement that does not exist when f(x) is expanded in a Taylor series about its mean value. However, as discussed in Section B.3, approximations can often be made for the probability density function such that the resulting statistical approximation for f(x) is considerably more accurate than the Taylor series, from a statisiical point of view.

Statistical Linearization--The Vector Case – We now seek a linear approximation for a vector function $\underline{f}(\underline{x})$ of a vector random variable $\underline{x}$, having probability density function $p(\underline{x})$. Following the statistical approximation technique outlined for the scalar case, we propose to approximate $\underline{f}(\underline{x})$ by the expression

$$\underline{f}(x) \cong \underline{a} + N_f \underline{x} \qquad \text{(B.2-20)}$$

where $\underline{a}$ and N_f, are a vector and a matrix to be determined. Defining the error

$$\underline{e} \triangleq \underline{f}(\underline{x}) - \underline{a} - N_f \underline{x} \qquad \text{(B.2-21)}$$

$\underline{a}$ and N_f are chosen so that the quantity

$$J = E[\underline{e}^T A \underline{e}] \qquad \text{(B.2-22)}$$

is minimized for some symmetric positive semidefinite matrix A. Substituting Eq. (B.2-21) into Eq. (B.2-22) and setting the partial derivative of J with respect to the elements of $\underline{a}$ equal to zero, we obtain

$$E[A(\underline{f}(x) - \underline{a} - N_f \underline{x})] = 0 \qquad \text{(B.2-23)}$$

Therefore, $\underline{a}$ is given by

$$\underline{a} = \hat{\underline{f}}(\bar{x}) - N_f \hat{\underline{x}} \qquad \text{(B.2-24)}$$

Substituting $\underline{a}$ from Eq. (B.2-24) into J and taking the partial derivative with respect to the elements of N_f yields

$$E\left[A\left[N_f \underline{x}\,\underline{x}^T + (\hat{\underline{f}}(\underline{x}) - \underline{f}(\underline{x}))\,\tilde{\underline{x}}^T\right]\right] = 0 \qquad \text{(B.2-25)}$$

where

$$\tilde{\underline{x}} = \underline{x} - \hat{\underline{x}}$$

Solving Eq. (B.2-25) produces

$$N_f = \left[\underline{\hat{f}}\,\underline{x}^T - \underline{\hat{f}}\,\hat{\underline{x}}^T\right] P^{-1} \qquad \text{(B.2-26)}$$

where P is the covariance matrix of $\underline{x}$. Observe that both $\underline{a}$ and N_f as given by Eqs. (B.2-24) and (B.2-26) are independent of the weighting matrix A; hence, they provide a generalized minimum mean square error approximation to $\underline{f}$.

Upon substitution from Eq. (B.2-24) into Eq. (B.2-20) we obtain

$$\underline{f}(\underline{x}) = \hat{\underline{f}}(\underline{x}) + N_f(\underline{x} - \hat{\underline{x}}) \qquad \text{(B.2-27)}$$

which is the form specified in Eq. (B.2-3). The quantity N_f is called the describing function matrix; as expected, N_f reduces to n_i in Eq. (B.2-12) when $\underline{x}$ and $\underline{f}$ are scalars. Because N_f is potentially a function of both the mean and covariance of $\underline{x}$, denoted by $N_f(P, \hat{\underline{x}})$, equations (B.2-5) and (B.2-7) become a set of coupled nonlinear differential equations;

$$\dot{\hat{\underline{x}}}(t) = \hat{\underline{y}}(t)$$

$$\dot{P}(t) = N_f(P, \hat{\underline{x}})\, P + P N_f(P, \hat{\underline{x}})^T + Q(t) \qquad \text{(B.2-28)}$$

B.3 COMPUTATION OF DESCRIBING FUNCTIONS

In order to carry out the integration of Eq. (B.2-28), it is necessary to compute $\hat{\underline{y}}(t)$ and $N_f(t)$. From the discussion in Section B.2, we know that

$$\hat{\underline{y}}(t) = \hat{\underline{f}}(t)$$

$$N_f(t) = [\widehat{\underline{f}\underline{x}^T} - \hat{\underline{f}}\,\hat{\underline{x}}^T]\, P^{-1} \qquad \text{(B.3-1)}$$

where $\hat{\underline{x}}$ and P are the mean and covariances of $\underline{x}(t)$, respectively and

$$\hat{\underline{f}} = \int_{-\infty}^{\infty} \underline{f}(\underline{x})\, p(\underline{x})\, d\underline{x}$$

$$\widehat{\underline{f}\underline{x}^T} = \int_{-\infty}^{\infty} \underline{f}(\underline{x})\, \underline{x}^T\, p(\underline{x})\, d\underline{x} \qquad \text{(B.3-2)}$$

Thus $\underline{x}$ and P can be continuously evaluated if the probability density function $p(\underline{x})$ in Eq. (B.3-2) is known.

Generally speaking, it is not practical to analytically evaluate the probability density function for the state of a nonlinear dynamical system; therefore an approximate form of $p(\underline{x})$ must be obtained. One frequently used assumption is that $\underline{x}$ is gaussion:

$$p(\underline{x}) \cong (2\pi \mathrm{Det}\,(P))^{-n/2} \exp\left[-\frac{1}{2}(\underline{x}-\hat{\underline{x}})^T P^{-1}(\underline{x}-\hat{\underline{x}})\right] \qquad \text{(B.3-3)}$$

This is based upon the fact that the states of the nonlinear system are the result of integrating the quantity $\underline{f}(\underline{x}) + \underline{w}$. Therefore $\underline{x}(t)$ is a linear superposition of past values of random quantities, which will tend to be gaussion even through $\underline{f}(\underline{x})$ and $\underline{w}$ may not be nongaussian. The latter assertion is based on qualitative application of the central limit theorum (Ref. 8). If Eqs. (B.3-2) and (B.3-3) are combined with Eq. (B.2-28), $\hat{\underline{x}}(t)$ and P (t) can be evaluated numerically on a digital computer.

From the above discussion, it is clear that more computation is required in applying covariance analysis techniques to nonlinear systems than for linear systems, because of the procedure used to evaluate $\hat{f}$ and N_f. Consequently, efficient means for calculating the right hand sides of Eq. (B.3-2) are desired. One useful simplification arises when the nonlinear system consists of a few single-state-input single-output nonlinearities, such as that illustrated in Fig. B.3-1. In this case, making the gaussion assumption described above, each nonlinear operation is replaced by its mean value and its describing function gain as indicated in Fig. B.2-1, both of which are scalars computed according to Eq. (B.2-12). Then the first-order vector and matrix differential equations in Eqs. (B.2-28) can be formulated by inspection of the resulting linear system block diagram. Thus the CADET equations can be constructed using existing tabulated describing functions for single-input

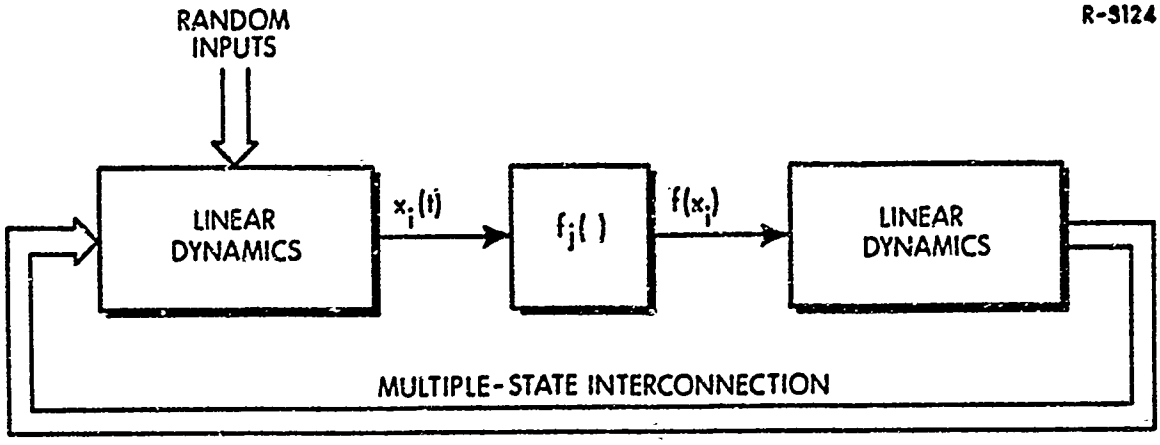

Figure B.3-1 Example of a Single-State-Input Single-Output Nonlinearity

single-output nonlinearities (Ref. 12). The proof of this assertion follows from the fact that $\hat{\underline{f}}$ and N_f are related by

$$N_f(t) = \frac{\partial \hat{\underline{f}}\,(\underline{x}(t))}{\partial\, \hat{\underline{x}}} \qquad \text{(B.3-4)}$$

where $\underline{x}$ is assumed to be a gaussian random variable. Eq. (B.3-4) is derived in Ref. 13. In the case of a single nonlinearity, as in Fig. B.3-1, the system equations can be written in the form

$$\dot{\underline{x}} = F\underline{x} + \begin{bmatrix} 0 \\ \vdots \\ 0 \\ f_j(x_i) \\ 0 \\ \vdots \\ 0 \end{bmatrix} \qquad \text{(B.3-5)}$$

where the term $F\underline{x}$ describes the dynamics of the linear part of the system. Applying Eq. (B.3-4), we have

$$N_f = \frac{\partial}{\partial \hat{\underline{x}}} \left\{ F\hat{\underline{x}} + \begin{bmatrix} 0 \\ \vdots \\ 0 \\ \hat{f}_j(x_i) \\ 0 \\ \vdots \\ 0 \end{bmatrix} \right\} \tag{B.3-6}$$

$$= F + \begin{bmatrix} 0 & \cdots & 0 & \cdots & 0 \\ \vdots & & \vdots & & \vdots \\ 0 & \cdots & 0 & \cdots & 0 \\ \vdots & & \vdots & & \vdots \\ 0 & \cdots & \dfrac{\partial \hat{f}_j}{\partial \hat{x}} & \cdots & 0 \\ \vdots & & \vdots & & \vdots \\ 0 & \cdots & 0 & \cdots & 0 \\ \vdots & & \vdots & & \vdots \\ 0 & \cdots & 0 & \cdots & 0 \end{bmatrix}$$

The term $\partial \hat{f}_j / \partial \hat{x}_i$ is simply the describing function gain for f_j, as determined by the statistics of its input, x_i; thus N_f is determined by the dynamics (F) of the linear system and the single-input describing gain. The extension of the above argument to the case when several single-state-input nonlinearities exist is straightforward.

B.4 MIXED CONTINUOUS-DISCRETE SYSTEMS

Preceeding sections of this appendix have treated continuous nonlinear systems; i.e., those governed by differential equations. However, in many practical applications, the system may include a digital computer whose input and output are expressed in terms of difference equations, as illustrated in Fig. B.4-1. Such a structure

arises in missile guidance systems where digital control laws are used to command the missile's maneuvering acceleration. In this section, equations are developed for propagating the mean and covariance of a nonlinear, mixed continuous-discrete system.

The equations of motion for a system of the type shown in Fig. B.4-1 are written in mixed differential-difference equation format. First of all, between sampling intervals the digital computer is effectively idle and the continuous part of the system satisfies an equation of the form

$$\left.\begin{aligned} \dot{\underline{x}}_c(t) &= \underline{f}(\underline{x}_c(t)) + \underline{g}(\underline{x}_d(t)) + \underline{w}(t) \\ \dot{\underline{x}}_d(t) &= \underline{0} \end{aligned}\right\} \quad t_k \le t < t_{k+1} \qquad \text{(B.4-1)}$$

where $\underline{x}_c(t)$ refers to the continuously varying states in the system, and $\underline{x}_d(t)$ is a collection of digital states (e.g., states in the digital computer) which remain unchanged during the sampling interval. Assuming that the composite state vector, $\underline{x}$, defined by

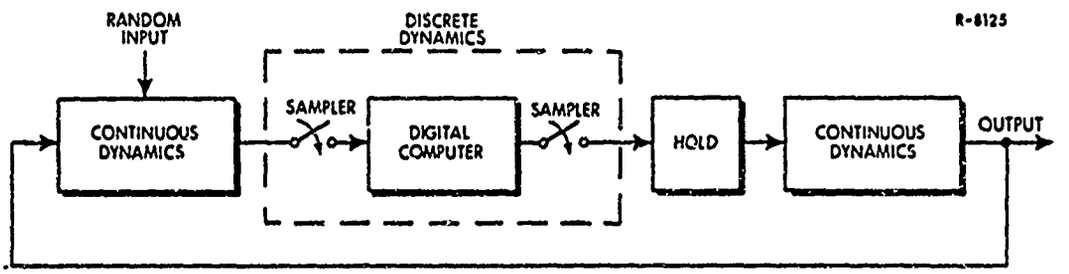

Figure B.4-1 An Example of a Mixed Continuous Discrete System

$$\underline{x} = \begin{bmatrix} \underline{x}_c \\ \underline{x}_d \end{bmatrix}$$

is gaussian with its mean and covariance matrix known at time t_k, then its statistics during the sampling interval can be calculated using

$$\frac{d}{dt}\begin{bmatrix} \hat{\underline{x}}_c(t) \\ \hat{\underline{x}}_d(t) \end{bmatrix} = \left[\hat{\underline{f}}(\underline{x}_c(t)) + \hat{\underline{g}}(\underline{x}_d)\right]; \quad t_k \le t < t_{k+1}$$

$$\dot{P}(t) = \begin{bmatrix} N_f(t) & N_g \\ 0 & 0 \end{bmatrix} P(t) + P(t) \begin{bmatrix} N_f(t)^T & 0 \\ N_g^T & 0 \end{bmatrix} + \begin{bmatrix} Q(t) & 0 \\ 0 & 0 \end{bmatrix}$$

$$t_k \le t < t_{k+1} \qquad \text{(B.4-2)}$$

where N_f and N_g are the describing function gain matrixes associated with $\underline{f}$ and $\underline{g}$ respectively. Observe that N_g remains constant throughout the sampling interval because $\underline{x}_d$ is itself constant.

Now, at a sampling interval, the digital computer performs a calculation which can be represented as a difference equation of the form

$$\begin{bmatrix} \underline{x}_c(t_{k+1}^+) \\ \hline \underline{x}_d(t_{k+1}^+) \end{bmatrix} = \begin{bmatrix} \underline{x}_c(t_{k+1}^-) \\ \hline \underline{h}\left(\underline{x}_c(t_{k+1}^-),\ \underline{x}_d(t_{k+1}^-)\right) \end{bmatrix} + \begin{bmatrix} 0 \\ \hline \underline{w}_{k+1} \end{bmatrix} \qquad \text{(B.4-3)}$$

where the superscript (-) denotes the solution to Eq. (B.4-1) just before the sampling instant and (+) denotes the new values of the state variables

just after a sampling instant. The vector $\underline{w}_{k+1}$ represents a random quantity that can enter the digital calculation as a result of instrument measurement noise. It is assumed that $\underline{w}_{k+1}$ has zero mean and covariance matrix Q_{k+1}. Observe that in Eq. (B.4-3) $\underline{x}_c$ remains unchanged because only the digital states can change instantaneously in time.

Because the mean and covariance of $\underline{x}_c$ and $\underline{x}_d$ at t_{k+1}^- are known from Eq. (B.4-2), the describing function gain matrix H_h corresponding to $\underline{h}$ in Eq. (B.4-3) can be evaluated. Thus we can rewrite Eq. (B.4-3) approximately as

$$\underline{x}_c(t_{k+1}^+) = \underline{x}_c(t_{k+1}^-)$$

$$\underline{x}_d(t_{k+1}^+) \cong \hat{\underline{h}} + H_h\left(\underline{x}(t_{k+1}^-) - \hat{\underline{x}}(t_{k+1}^-)\right) + \underline{w}_{k+1} \tag{B.4-4}$$

From Eq. (B.4-4) it follows that the mean and covariance of the system states just after the sample-time are given by

$$\hat{\underline{x}}(t_{k+1}^+) = \begin{bmatrix} \hat{\underline{x}}_c(t_{k+1}^+) \\ \hat{\underline{x}}_d(t_{k+1}^+) \end{bmatrix} = \begin{bmatrix} \hat{\underline{x}}(t_{k+1}^-) \\ \hat{\underline{h}}\left(\underline{x}_c(t_{k+1}^-),\ \underline{x}_d(t_{k+1}^-)\right) \end{bmatrix}$$

$$P(t_{k+1}^+) = \left[\begin{array}{c|c} I & 0 \\ \hline H_h & \end{array}\right] P(t_{k+1}^-) \left[\begin{array}{c|c} I & \\ \hline 0 & H_h^T \end{array}\right] + \left[\begin{array}{c|c} 0 & 0 \\ \hline 0 & Q_k \end{array}\right] \tag{B.4-5}$$

After evaluating Eqs.(B.4-5), $\underline{x}(t_{k+1}^+)$ and $P(t_{k+1}^+)$ are the initial conditions for propagating the mean and covariance over the next

sampling interval using Eqs. (B.4-2). Thus by alternately evaluating the differential and difference propagation equations, the mean and covariance matrix of the mixed continuous-discrete nonlinear system can be evaluated.

B.5 DESCRIBING FUNCTIONS FOR SATURATION AND SINUSOIDAL NONLINEARITIES

Describing functions for the saturation and sinusoidal nonliniarities in Fig. 2.1-2 are calculated in Ref. 12 for gaussian inputs. These are shown graphically in Figs. B.5-1 and B.5-2. The exact analytical expressions are as follows:

Saturation

$$n(\sigma) = m\left[2\,PI\left(\frac{\delta}{\sigma}\right) - 1\right]$$

$$PI\left(\frac{\delta}{\sigma}\right) = \frac{1}{\sqrt{2\pi}}\int_{-\infty}^{\delta/\sigma} \exp\left[-\frac{v^2}{2}\right] dv \qquad \text{(B.5-1)}$$

Sinusoidal

$$n(\sigma) = Mme^{-m^2\sigma^2/2} \qquad \text{(B.5-2)}$$

Equation (B.5-1) contains a term, $PI\left(\frac{\delta}{\sigma}\right)$, which is the integral of the gaussian density function, sometimes called a probability integral. The latter cannot be expressed in closed form. However, an approximate expression which is accurate to one part in 10^{-5} is given by (Ref. 14)

$$PI\left(\frac{\delta}{\sigma}\right) \cong 1 - \left\{\frac{1}{\sqrt{2\pi}} \exp\left[-\frac{\delta^2}{2\sigma^2}\right]\right\} \sum_{i=1}^{3} a_i w^i$$

$$w = \frac{1}{1 + \frac{b\delta}{\sigma}}$$

$$b = 0.33267 \qquad a_2 = -0.1201676$$

$$a_1 = 0.4361836 \qquad a_3 = 0.9372980 \qquad \text{(B.5-3)}$$

Equations (B.5-1) through (B.5-3) are used to calculate the describing function gains in the CADET simulation.

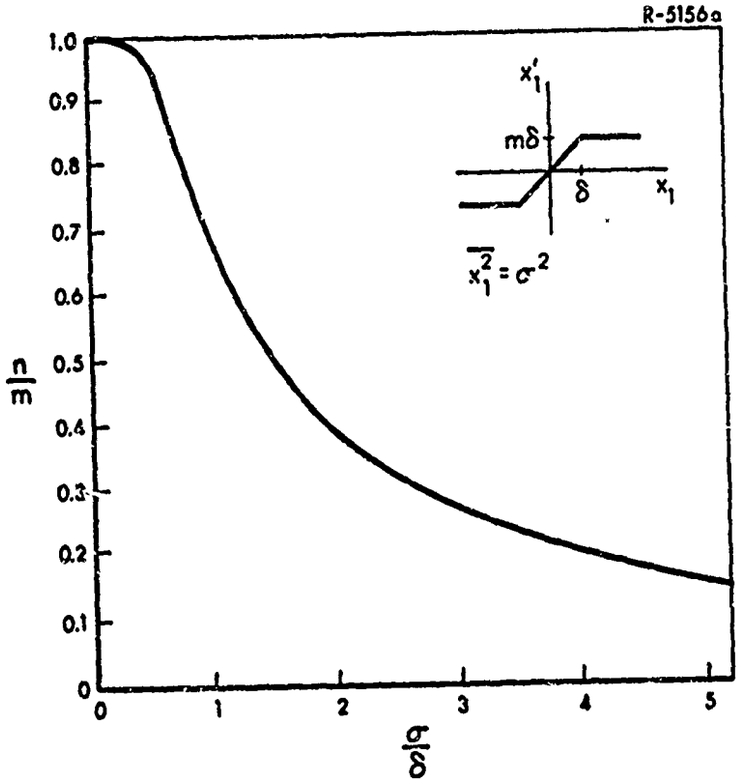

Figure B.5-1 Describing Function for Saturation with a Gaussian Input

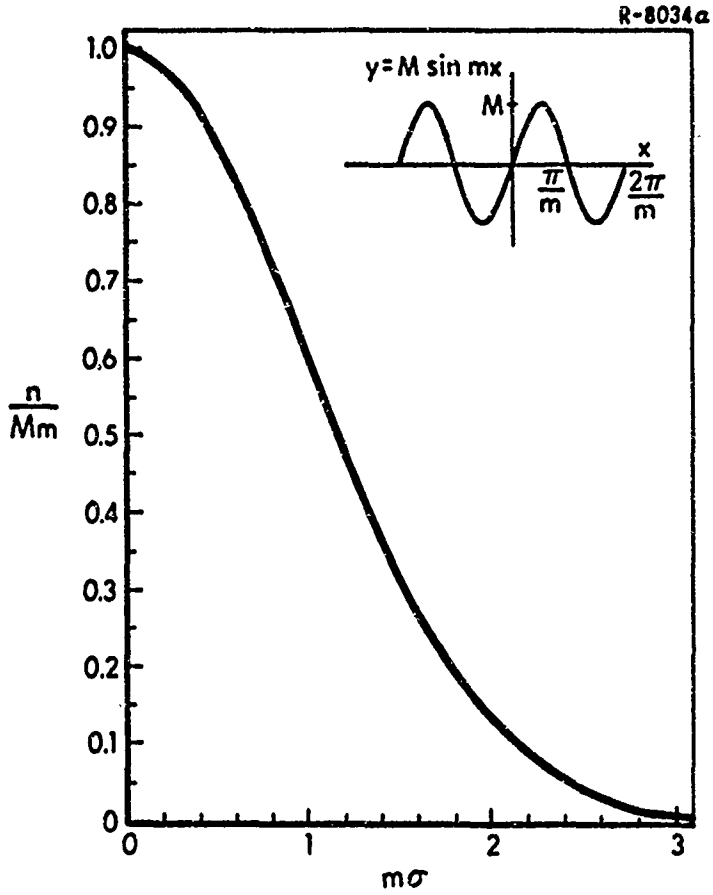

$$N = Mme^{-m^2\sigma^2/2}$$

Figure B.5-2 Describing Function for a Sinusoid with a Gaussion Input

REFERENCES

1. James, J.P., "Homing Guidance," A-62-1732.3-68, Aerospace Corporation, September 14, 1962.

2. Willems G., "Optimal Controllers for Homing Missiles", Report No. RE-TR-68-15, U.S. Army Missile Command, Redstone Arsenal, Alabama, September 1968.

3. Stallard, D.V., "Classical and Modern Guidance of Homing Interceptor Missiles," P247, April 1968, Raytheon Company, Missile Systems Division, Bedford, Massachusetts.

4. Garber, V., "Optimum Intercept Laws for Accelerating Targets," AIAA Journal Vol. 6, No. 11, November 1968.

5. Price, C.F., "Adaptive Control and Guidance for Tactical Missiles," Vol. II, The Analytic Sciences Corporation, TR-170-1, 30 June 1970.

6. Gelb, A., and Warren, R.S., "Direct Statistical Analysis of Nonlinear Systems--CADET," Paper No. 72-875, AIAA Guidance and Control Conference, Stanford, California, August 1972.

7. Price, C.F., "Optimal Stochastic Guidance Laws for Tactical Missiles", TR-170-2, The Analytic Sciences Corporation, 1 September 1971.

8. Sage, A.P., Optimum Systems Control, Prentice-Hall, Inc., Englewood Cliffs, N.J., 1968.

9. Davenport, W.B., Jr., and Root, W.L., Random Signals and Noise, McGraw-Hill Book Co., New York, 1958.

10. Bryson, A.E., Jr., and Ho, Y.C., Applied Optimal Control, Blaisdell Publishing Co., Waltham, Massachusetts, 1969.

11. Deyst, J.J., Jr., and Price, C.F., "Optimal Stochastic Guidance Laws for Tactical Missiles," to be published, AAIA Journal on Spacecraft and Rockets

12. Gelb, A., and Vander Velde, W.E., Multiple-Input Describing Functions and Nonlinear Systems Design, McGraw-Hill Book Co., New York, 1968.

13. Phaneuf, R.J., "Approximate Nonlinear Estimation," Ph.D. Thesis, Dept. of Aeronautics and Astronautics, M.I.T., Cambridge, Mass., May 1968.

14. Abramowitz, M., and Stegun, I.A. (editors), Handbook of Mathematical Functions with Formulas, Graphs, and Mathematical Tables, No. 55 in National Bureau of Standards Applied Mathematics Series, U.S. Department of Commerce, Washington, D.C., 1964.

15. Mendel, J.M., "Computational Requirements for a Discrete Kalman Filter," IEEE Transactions on Automatic Control, Vol. AC-16, No. 6, December 1971.